

## Effective dynamic mass density of composites

Jun Mei,<sup>1</sup> Zhengyou Liu,<sup>2</sup> Weijia Wen,<sup>1</sup> and Ping Sheng<sup>1</sup>

<sup>1</sup>*Department of Physics, Hong Kong University of Science and Technology, Clear Water Bay, Kowloon, Hong Kong, China*

<sup>2</sup>*Department of Physics, Wuhan University, Wuhan 430072, China*

(Received 2 May 2007; revised manuscript received 22 June 2007; published 16 October 2007)

The static mass density of a composite is simply the volume average of its constituents' densities. The dynamic density of a composite is defined to be the quantity that enters in evaluating the elastic wave velocity at the low-frequency limit. We show through a rigorous derivation that the effective dynamic mass density of an inhomogeneous mixture can differ from its static counterpart when the composite matrix is a fluid or, more generally, when there are relative motions between the matrix and inclusions. Derivation of the dynamic mass density expressions, involving taking the long wavelength limit of the rigorous multiple scattering theory, is detailed for the two-dimensional case. We also extend the effective dynamic mass density expression to finite frequencies where there can be low-frequency resonances. By combining both analytical and numerical approaches, negative or complex dynamic mass density is obtained for composites that contain a sufficient fraction of locally resonant inclusions. Thus, the dynamic mass density of a composite can differ from the static (volume-averaged) value even in the zero frequency limit, although both must be positive in that limit. Negative or complex dynamic mass density can occur at finite frequencies. These two results are shown to be consistent with each other, as well as related by the same underlying physics. As by-products of our rigorous derivation, we also verify some prior known results on the effective elastic moduli of composites.

DOI: [10.1103/PhysRevB.76.134205](https://doi.org/10.1103/PhysRevB.76.134205)

PACS number(s): 43.35.+d, 43.20.+g, 43.40.+s

### I. INTRODUCTION

Recent excitement on metamaterials has cast attention on the seemingly mundane subject of composite mass density. This is because for the electromagnetic metamaterials, a negative index of refraction is realized when both the dielectric constant  $\epsilon$  and magnetic permeability  $\mu$  are negative. If there are corresponding acoustic metamaterials, then both the elastic modulus and mass density should be negative. However, can the mass density be negative? The static mass density  $\rho_{eff}$  of a composite can never be negative since it must be equal to the volume average of its constituents' densities. However, for metamaterials, the relevant density  $D_{eff}$  is that used in calculating the acoustic wave velocity  $V = \sqrt{B_{eff}/D_{eff}}$ , where  $B_{eff}$  denotes the effective bulk modulus. The relevant question is: Does  $\rho_{eff} = D_{eff}$  always? The conventional wisdom says "yes," at least in the low-frequency limit. However, what we would like to show in this work is that the answer is actually "no"; i.e., the static and dynamic mass densities can differ in certain cases even in the low-frequency limit. Moreover, by extending the dynamic mass density expression to finite frequencies, we show that it can actually be negative or complex as well. Hence, acoustic metamaterials are potentially realizable.

Below, we recapitulate the prior and contemporary works on this topic in Sec. II, followed in Sec. III by a statement of main results. In Sec. IV, we present the rigorous derivation of the effective dynamic mass density expression in two-dimensional (2D) composites by taking the long wavelength limit of the multiple scattering theory (MST). It will be shown that depending on whether the composite matrix is fluid or solid, the resulting effective dynamic density expression can be different. The derived mass density expression is used to explain some recent experimental data in Sec. V, from which a physical understanding of the different mass density expression emerges. In Sec. VI, we extend the effective

dynamic mass density expression to finite frequencies and show that when there exist low-frequency local resonances, the effective dynamic density can be complex in general and negative in some particular frequency regimes. This holds true for composites with either solid or fluid matrix. In Sec. VII, we conclude by addressing the relevance of our results to acoustic metamaterials. In order not to interrupt the main line of exposition, the more tedious algebraic derivation steps are given in the appendixes.

### II. RECAPITULATION

More than 30 years ago, in the study of seismic wave propagation in two-phase media, Kuster and Toksöz<sup>1</sup> found a surprising result that the effective dynamic mass density  $D$  of a three-dimensional composite is not the same as the intuitive volume-averaged mass density (VAMD),  $\rho$ , provided the composite matrix is fluid. Ten years later, in studying the wave properties of composites in the long wavelength limit, Berryman<sup>2</sup> also derived the effective dynamic mass density expression by using both the average  $T$  matrix approximation and the coherent potential approximation (CPA). He obtained the same result—that the dynamic mass density is not equal to the static mass density for the fluid-matrix composites, while for composites with the solid matrix, the two are the same. However, these results were greeted mostly with curiosity, in part because of the strong feeling within the community that the volume-averaged density is unique, at least in the long wavelength limit, and in part also because there has been no experimental support for the validity of the alternative mass density expression. The fact that the derivation was nonrigorous also contributed to the lack of confidence in deviating from the VAMD.

Recently, the proposal and realization of locally resonant sonic materials (LRSMs),<sup>3,4</sup> consisting of hard spheres coated with soft cladding and dispersed in a stiff host me-

dium, have shown experimentally that the LRSM can display a negative effective response in certain frequency regimes, at frequencies where the relevant wavelengths in the matrix are 2 orders of magnitude larger than the feature sizes. Such negative responses can be attributed to either negative effective modulus or negative effective mass density. Subsequently, in Ref. 5, an analytic model was constructed to show that around the locally resonant frequencies, the effective mass density of the LRSM is negative, thus providing the first support to the fact that effective dynamic mass density can be not only different from, but also opposite in sign from the static mass density. However, that still leaves open the question: Are the conclusions of Kuster and Toksöz and Berryman correct in the limit of zero frequency?

In a recent paper,<sup>6</sup> we resolved that question by using the rigorous MST to derive the Berryman mass density expression, and explained the experimental data by Cervera *et al.*<sup>7</sup> on that basis. Thus, we have established unambiguously that the effective dynamic mass density can be different from the static one at the long wavelength (or zero frequency) limit. Moreover, the extension to finite frequencies can directly lead to the results, as previously evidenced by LRSM. Contemporary with our work, Milton and Willis<sup>8</sup> reported their finding that the effective mass density of a composite at any given frequency is, in general, a second-order tensor if the composite is inhomogeneous on a length scale smaller than the scale of practical observation. In addition, Ávila *et al.*<sup>9</sup> studied an elastic matrix containing very compliant inclusions and also found that the effective mass density can be frequency dependent and anisotropic.

Related to the effective dynamic mass density is the effective bulk modulus. The recent work of Fang *et al.* has shown that by using Helmholtz resonators (HRs), the effective bulk modulus can indeed turn negative in certain frequencies.<sup>10</sup> Thus, by combining the LRSM with the HR, it is possible that the acoustic metamaterials can be realized, with all the attendant novel characteristics.

### III. STATEMENT OF MAIN RESULTS

The main purpose of this work is to provide a coherent and unified account of the dynamic mass density issue. In particular, we present (1) the justification and detailed rigorous derivation of the dynamic mass density expressions, putting on a firm basis some of the previously known results; (2) a comparison with experiment and the accompanying physical understanding of the dynamic mass density that emerges; and (3) the extension of the dynamic mass density expression to the finite frequency regime where there can be low-frequency local resonances, so as to establish the link to locally resonant sonic materials.

The dynamic mass density of composites at the zero frequency limit depends crucially on whether the matrix is fluid or solid. For the fluid matrix, the dynamic mass density is the Berryman mass density, i.e.,

$$D_{eff} = \frac{(D_2 + D_1) + (D_2 - D_1)f}{(D_2 + D_1) - (D_2 - D_1)f} D_1,$$

while for the solid matrix, the dynamic mass density is the same as the static VAMD, i.e.,  $D_{eff} = \rho_{eff} = (1-f)D_1 + fD_2$ .

As by-products of our derivation, we also verify some prior known results on the effective Lamé constants of composites. For the fluid-matrix composites, the effective bulk modulus is the harmonic average of its constituents' bulk moduli, i.e.,

$$\frac{1}{B_{eff}} = \frac{1-f}{B_1} + \frac{f}{B_2}.$$

For the solid-matrix composites, the effective elastic moduli are given by

$$\frac{\mu_{eff} - \mu_1}{\mu_{eff} + \mu_1} = f \frac{\mu_2 - \mu_1}{\mu_2 + \mu_1}$$

and

$$\frac{(\lambda_{eff} + \mu_{eff}) - (\lambda_1 + \mu_1)}{\lambda_{eff} + \mu_{eff} + \mu_1} = f \frac{(\lambda_2 + \mu_2) - (\lambda_1 + \mu_1)}{\lambda_2 + \mu_2 + \mu_1}.$$

At finite frequencies, the dynamic mass density is closely related to the scattering coefficient of the embedded inclusions. For the fluid-matrix composites, the dynamic mass density is given by

$$\frac{D_{eff} - D_1}{D_{eff} + D_1} = \frac{4f}{i\pi(\alpha_1 r)^2} S_1(1),$$

where  $S_1(1) = T_{11}$  is the  $n=1$  angular channel Mie scattering coefficient for the inclusion in the longitudinal mode, with  $\alpha_1$  being the longitudinal wave number in the fluid matrix, and  $f$  and  $r$  being the filling ratio and radius of the (cylindrical) inclusions, respectively. Here,  $S_1(1) = T_{11}$  is defined by Eqs. (11) and (36). For the solid-matrix composites, the dynamic mass density is determined by

$$\frac{D_{eff}}{D_1} - 1 = \frac{4f}{i\pi(\beta_1 r)^2} \frac{b_{03}(1)}{a_{03}(1)},$$

where  $b_{03}(1)/a_{03}(1) = T_{03,03}$  is the  $n=0$  angular channel Mie scattering coefficient for the inclusion in the transverse mode, with  $\beta_1$  being the transverse wave number in the solid matrix. Here,  $b_{03}(1)/a_{03}(1) = T_{03,03}$  is defined by Eqs. (49) and (50).

Similarly, the effective bulk modulus of the fluid-matrix composites at finite frequencies is given by

$$-1 + \frac{B_1}{B_{eff}} = \frac{4f}{i\pi(\alpha_1 r)^2} S_0(1),$$

where  $S_0(1) = T_{00}$  is the  $n=0$  angular channel Mie scattering coefficient for the inclusion in the longitudinal mode, defined by Eqs. (11) and (36).

For the solid-matrix composites, the effective Lamé constants are determined by

$$\frac{\mu_{eff} - \mu_1}{\mu_{eff} + \mu_1} = \frac{4if}{\pi(\beta_1 r)^2} \frac{b_{13}(1)}{a_{13}(1)}$$

and

$$\frac{(\lambda_{eff} + \mu_{eff}) - (\lambda_1 + \mu_1)}{\lambda_{eff} + \mu_{eff} + \mu_1} = \frac{4if}{\pi(\alpha_1 r)^2} \frac{b_{01}(1)}{a_{01}(1)},$$

where  $b_{13}(1)/a_{13}(1) = T_{13,13}$  is the  $n=1$  angular channel Mie scattering coefficient for the inclusion in the transverse mode and  $b_{01}(1)/a_{01}(1)$  is the  $n=0$  angular channel Mie scattering coefficient for the inclusion in the longitudinal mode. Here,  $b_{13}(1)/a_{13}(1) = T_{13,13}$  and  $b_{01}(1)/a_{01}(1)$  are defined by Eqs. (49) and (50).

By taking the zero frequency limits of the finite frequency expressions, we have obtained consistency with the respective independently derived, long wavelength limit expressions for the dynamic mass density and elastic moduli.

By using the multiple scattering theory to numerically evaluate the scattering cross sections at finite frequencies, we obtained the effective dynamic mass densities for the LRSM composites. It is shown in Figs. 7 and 9 that in the vicinities of the local resonances, the dynamic mass density can be complex in general and negative in particular frequency regions. The finite frequency elastic moduli of LRSM can be similarly evaluated.

#### IV. EFFECTIVE DYNAMIC MASS DENSITY IN THE LONG WAVELENGTH LIMIT

In this section, we use the rigorous MST to derive the effective dynamic mass density expression. MST can be exact because it considers periodic structures. Its application to random composites is made possible by the fact that in the limit of zero frequency (or the long wavelength limit), the dispersion relation (the  $\omega$ - $k$  relation) must be linear with a slope (indicative of the effective wave speed) that depends only on the relative volume fraction (or area fraction for 2D composites) of the composite constituents. In other words, provided the lattice structure or arrangement of the scatterers preserves the isotropy requirement (for the anisotropic case, see below), structural considerations enter only as higher-order terms in our low-frequency expansions; hence, the effective wave speed obtained is independent of whether the composite is periodic or random, at least to the leading order. However, such an approach, of course, has its limitations in that the random composite should not have long-range correlated microstructures, e.g., percolating clusters, that are absent in the original periodic system. This point is emphasized below.

In order to be self-contained, we briefly justify (1) the linear dispersion relation in the long wavelength limit and (2) that the slope should be the same for either the periodic or random composites. Details can be found in Ref. 11.

Consider the scalar wave equation for an isotropic, inhomogeneous composite,

$$\nabla^2 \phi + \frac{\omega^2}{c^2(\vec{x})} \phi = 0, \quad (1)$$

in which  $\omega$  denotes angular frequency and  $c = \sqrt{B/\rho}$  is the local wave speed, where  $B$  is the bulk modulus and  $\rho$  the

static mass density of the constituent at position  $\vec{x}$ . Equation (1) can be rearranged into a form

$$\nabla^2 \phi + \frac{\omega^2}{c_0^2} \phi = \frac{\omega^2}{c_0^2} \left( 1 - \frac{c_0^2}{c^2(\vec{x})} \right) \phi, \quad (2)$$

where the right-hand side denotes the scattering source, and  $c_0$  is the wave speed of the matrix material, or the value suitably determined by, e.g., the CPA (or its extension to the intermediate frequency regime).<sup>11</sup> It is important to note that for the classical waves, the scattering source strength is proportional to  $\omega^2$ , as indicated by the right-hand side of Eq. (2). In particular, it implies that scattering vanishes as  $\omega \rightarrow 0$ , as evidenced by the frequency dependence of the Rayleigh scattering cross section. From Eq. (2), one can obtain for a random composite the configurationally averaged Green's function in the wave vector representation,

$$\langle G \rangle_c = \frac{1}{(\omega^2/c_0^2) - k^2 - \Sigma(\omega, k)}, \quad (3)$$

where  $k$  is the magnitude of the wave vector,  $\langle \rangle_c$  denotes configurational averaging over random configurations with the same statistics,  $G$  is the Green's function, and  $\Sigma$  denotes the self-energy that arises from multiple scattering [owing to the nonzero right-hand side of Eq. (2)]. Equation (3) is formally rigorous; no approximation is involved. Due to the fact that the scattering source strength is proportional to  $\omega^2$ , it can be shown explicitly that in the limit of  $\omega \rightarrow 0$ , the leading-order term for  $\Sigma$  is proportional to  $\omega^2$ . That is,  $\Sigma \cong \Sigma_0 \omega^2 + \dots$ . In addition, if  $\Sigma_0$  exists (as implied by the existence of the CPA solution), then in the long wavelength limit it must be independent of  $k$ . This is because, physically, the wave vector dependence arises from spatial correlations (i.e., spatial derivatives), and in the long wavelength limit the scattering becomes point-particle-like (and multiple scatterings are inherently higher order); hence, to the leading order, it contains no information on correlations and is therefore independent of  $k$ . As a consequence, in the long wavelength limit, Eq. (3) becomes

$$\langle G \rangle_c \cong \frac{1}{(\omega^2/V_{eff}^2) - k^2}, \quad (4a)$$

with

$$V_{eff}^2 = \frac{c_0^2}{1 - \Sigma_0 c_0^2}. \quad (4b)$$

Since the zero of the Green's function denominator directly yields the dispersion relation, Eqs. (4a) and (4b) tell us that, indeed, at the (low-frequency) long wavelength limit, the dispersion relation is always linear. The slope of that linear relation is independent of whether the system is periodic or random, although it does depend on the relative volume fraction (or area fraction for 2D composites) of the constituents.

It follows from the above discussions that we can take the rigorous MST, formulated for periodic composites, and take its long wavelength limit to obtain the effective wave speed

for either the periodic or random composites. In fact, for acoustic waves we have explicitly verified the wave speed to be independent of whether the lattice is hexagonal or square symmetry, at least to the leading order, as long as the area fraction of the inclusions is the same and the isotropy assumption is maintained. While the above considerations are for the scalar wave equation, its conclusions are generally valid for classical waves in general.

However, three caveats must be noted in the application of the above argument. First, if the system is anisotropic, which might arise from either the anisotropic arrangement (lattice for the periodic case) of isotropic scatterers or the anisotropy of the scatterers (e.g., ellipsoid instead of spheres), then  $\langle G \rangle_c$  can display anisotropy as well since the configurational averaging is only over the random placement of the structural units, hence preserving the anisotropic characteristics even after averaging. In that case, there can be different self-energy values along the different directions, giving rise to anisotropy in speeds. Second, in a random system it is often the case that if the scatterers are placed randomly, then there is necessarily a percolation threshold, i.e., a concentration at which the scatterers can form an infinitely connected network. What we describe here does not apply to systems where the scatterers can form percolation clusters. Instead, we require the scatterers to be separated by the matrix medium, no matter how high the concentration of scatterers. That is, we require the dispersion microstructure to be preserved, whether in periodic lattice or in random composites. Third, when the concentration of scatterers is very high (almost close packing), it is expected that higher-order terms in  $T^{-1}$  and  $G$  matrices would start to contribute a non-negligible part to the effective wave speed. It is physically reasonable that more angular channels are needed to accurately describe the situation when the scatterers almost touch each other. For such high concentrations, the effective sound speeds could be different between the square lattice and the hexagonal lattice; i.e., they become structure sensitive, although the effective sound speed itself is still isotropic for either lattice.

### A. Multiple scattering theory

We begin with a short description of the rigorous MST for two-dimensional phononic crystals.<sup>12</sup> For a time-harmonic wave, the elastic wave equation may be written as

$$\nabla \cdot \mu[\nabla \vec{u} + (\nabla \vec{u})^T] + \nabla(\lambda \nabla \cdot \vec{u}) + D\omega^2 \vec{u} = 0, \quad (5)$$

where  $D$  is the mass density,  $\lambda$  and  $\mu$  are the (spatially varying) Lamé constants,  $\vec{u}$  is the displacement vector, and  $(\nabla \vec{u})^T$  denotes the transpose of the tensorial quantity  $\nabla \vec{u}$ . MST represents a solution of the elastic wave equation [Eq. (5)] for a periodic composite that accounts fully for *all* the multiple scattering effects between any two scatterers, as shown schematically in Fig. 1, plus the inherent vector character of elastic waves. Thus, it is an exact theory without any approximation.

Before going directly to the details of the MST, it is meaningful to inspect the boundary conditions which will be

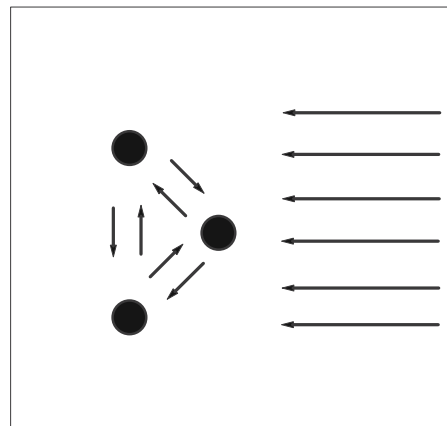


FIG. 1. Schematic diagram of the multiple scattering theory (MST).

used in our approach. For solid (cylinder) scatterers embedded in an inviscid fluid matrix, the elastic boundary condition requires that the tangential shear stress be zero at the interface between the scatterer and the fluid matrix. However, it is well known that for real fluid with a finite viscosity  $\eta$ , there is a thin fluid layer next to the interface where the viscosity effect dominates over the inertial effect. Waves will be exponentially attenuated in a fluid channel with width  $l$  if  $l$  is smaller than this viscous layer thickness. This is the viscous regime in ac permeability, where the Darcy law holds. However, if  $l > \sqrt{\eta/\rho\omega}$ , where  $\rho$  denotes the fluid density, then the inertial effect dominates and waves can propagate in the fluid channel *as though the fluid is inviscid*. This latter regime is assumed in our approach, which can be insured by letting viscosity  $\eta \rightarrow 0$ . Thus, in application to actual physical systems, we must check the condition  $\eta/\rho\omega l^2 \ll 1$  to be valid, where  $l$  is the minimum fluid channel width in the system. In Sec. V we show this condition to be indeed well satisfied in a recent experiment to which we compare our findings.

For our more specific case of 2D phononic crystals with a fluid matrix, MST has a rather simple form. In polar coordinates, the incident wave on scatterer  $i$  may be expressed generally as

$$\vec{u}_i^{in}(\vec{\rho}_i) = \sum_n a_n^i \vec{J}_n^i(\vec{\rho}_i) \quad (6)$$

and the wave scattered by scatterer  $i$  may be expressed as

$$\vec{u}_i^{sc}(\vec{\rho}_i) = \sum_n b_n^i \vec{H}_n^i(\vec{\rho}_i), \quad (7)$$

where the vector functions  $\vec{J}_n(\vec{\rho})$  and  $\vec{H}_n(\vec{\rho})$  are defined as

$$\begin{aligned} \vec{J}_n(\vec{\rho}) &= \nabla[J_n(\alpha_1 \rho) e^{in\varphi}], \\ \vec{H}_n(\vec{\rho}) &= \nabla[H_n(\alpha_1 \rho) e^{in\varphi}], \end{aligned} \quad (8)$$

with  $\alpha_1 = \omega \sqrt{D_1/\lambda_1}$  being the wave number in the fluid matrix,  $D_1$  and  $\lambda_1$  denoting the mass density and Lamé constant

of the matrix,  $\vec{\rho}=(\rho, \varphi)$  being the polar coordinates, and  $J_n(x)$  and  $H_n(x)$  on the right side of Eq. (8) denoting the  $n$ th Bessel function and Hankel function of the first kind, respectively. Since the incident wave on scatterer  $i$  comes from scattered waves by all the scatterers except  $i$  (for the purpose of calculating the dispersion relation, we do not need an externally incident wave), we have

$$\vec{u}_i^{in}(\vec{\rho}_i) = \sum_{j \neq i} \sum_{n''} b_{n''}^j \vec{H}_{n''}^j(\vec{\rho}_j), \quad (9)$$

where  $\vec{\rho}_i$  and  $\vec{\rho}_j$  refer to the position of the same spatial point measured from scatterers  $i$  and  $j$ , respectively. With  $\vec{R}_{i(j)}$  denoting the position of scatterer  $i(j)$ , we have proven that (see Ref. 12 for details)

$$\vec{H}_{n''}^j(\vec{\rho}_j) = \vec{H}_{n''}^j[\vec{\rho}_i - (\vec{R}_j - \vec{R}_i)] = \sum_n G_{n''n}^{ij} \vec{J}_n^i(\vec{\rho}_i), \quad (10)$$

where the structure constant  $G_{n''n}^{ij} = G_{n''n}(\vec{R}_j - \vec{R}_i) = H_{n-n''}(\alpha_1 |\vec{R}_j - \vec{R}_i|) e^{-i(n-n'')\phi}$  denotes the translation coefficients, with  $\phi = \arg(\vec{R}_j - \vec{R}_i)$ . There is a relation between the expansion coefficients  $\{a_n^j\}$  and  $\{b_n^j\}$ ,

$$b_n = \sum_{n'} T_{nn'} a_{n'}, \quad (11)$$

in which  $T = \{T_{nn'}\}$  is the elastic Mie scattering matrix<sup>12</sup> for a single scatterer. After substituting Eqs. (6), (10), and (11) into Eq. (9), we arrive at

$$\sum_{jn'} \left( \delta_{ij} \delta_{nn'} - \sum_{n''} G_{nn''}^{ij} T_{n''n'}^j \right) a_{n'}^j = 0. \quad (12)$$

For a periodical system, Eq. (12) may be Fourier transformed to

$$\sum_{n'} \left[ \delta_{nn'} - \sum_{n''} G_{nn''}(\vec{k}) T_{n''n'} \right] a_{n'} = 0, \quad (13)$$

where  $G_{nn''}(\vec{k}) = \sum_{\vec{R} \neq 0} G_{nn''}(-\vec{R}) \exp(i\vec{k} \cdot \vec{R})$ . The normal modes of the periodic system may be obtained by solving the following secular equation:

$$\det |T_{nn'}^{-1} - G_{nn''}(\vec{k})| = 0. \quad (14)$$

For the more general case of solid-matrix phononic crystals, the corresponding MST expressions can be found in Ref. 12.

### B. Fluid-matrix composites

By taking the low-frequency limit and retaining terms to the order of  $\omega^{-2}$ , both the  $T^{-1}$  matrix and the  $G$  matrix can be simplified to a  $3 \times 3$  matrix as follows (see Appendixes A and B for details):

$$T^{-1} = -I + \frac{4i}{\pi r^2} \frac{1}{\alpha_1^2} \begin{bmatrix} \frac{D_1 + D_2}{D_1 - D_2} & 0 & 0 \\ 0 & \frac{\lambda_2 + \mu_2}{\lambda_2 + \mu_2 - \lambda_1} & 0 \\ 0 & 0 & \frac{D_1 + D_2}{D_1 - D_2} \end{bmatrix} \quad (15)$$

and

$$G = -I + \frac{4i}{A} \frac{1}{1 - x^2} \frac{1}{\alpha_1^2} \begin{bmatrix} -x^2 & x e^{-i\theta_0} & e^{-2i\theta_0} \\ -x e^{i\theta_0} & -x^2 & x e^{-i\theta_0} \\ e^{2i\theta_0} & -x e^{i\theta_0} & -x^2 \end{bmatrix}. \quad (16)$$

In Eq. (15),  $r$  is the radius of the cylindrical inclusions, and

$$(T^{-1})_{00} = -1 + \frac{4i}{\pi r^2} \frac{1}{\alpha_1^2} \frac{\lambda_2 + \mu_2}{\lambda_2 + \mu_2 - \lambda_1}$$

is the low-frequency limit of the  $n=0$  angular channel scattering coefficient, while

$$(T^{-1})_{11} = -1 + \frac{4i}{\pi r^2} \frac{1}{\alpha_1^2} \frac{D_1 + D_2}{D_1 - D_2}$$

is the low-frequency limit of the  $n=1$  angular channel scattering coefficients. As evident in the expression of the  $T^{-1}$  matrix, the mass densities ( $D_1$  and  $D_2$ ) and the Lamé constants ( $\lambda_1$ ,  $\lambda_2$ , and  $\mu_2$ ) represent separate, yet at the same time parallel, wave scattering channels. In Eq. (16),  $A$  denotes the area of the unit cell and  $x = V_{eff}/V_1$  is the ratio of the effective sound velocity to the fluid-matrix sound velocity. It is the unknown to be evaluated.

By substituting Eqs. (15) and (16) into Eq. (14), the secular equation in the low-frequency limit is given by

$$\det \begin{bmatrix} \frac{D_1 + D_2}{D_1 - D_2} + \frac{x^2 f}{1 - x^2} & \frac{ixf}{1 - x^2} & -\frac{f}{1 - x^2} \\ -\frac{ixf}{1 - x^2} & \frac{B_2}{B_2 - B_1} + \frac{x^2 f}{1 - x^2} & \frac{ixf}{1 - x^2} \\ -\frac{f}{1 - x^2} & -\frac{ixf}{1 - x^2} & \frac{D_1 + D_2}{D_1 - D_2} + \frac{x^2 f}{1 - x^2} \end{bmatrix} = 0, \quad (17)$$

in which  $B_1 = \lambda_1$  and  $B_2 = \lambda_2 + \mu_2$  are the bulk moduli for the liquid matrix and the solid inclusions, respectively, while  $f = \pi r^2/A$  is the filling ratio of the solid inclusions. If we define dimensionless quantities  $M_0$  and  $M_1$  as

$$\begin{aligned} M_0 &= \frac{B_2}{B_2 - B_1}, \\ M_1 &= \frac{D_1 + D_2}{D_1 - D_2}, \end{aligned} \quad (18)$$

then the secular equation  $\det|T^{-1} - G| = 0$  is equivalent to the following equation:

$$(f - M_0)(f - M_1)x^4 + (fM_1 - f^2 - 2M_0M_1)x^2 + M_0(f + M_1) = 0. \quad (19)$$

If we further define the coefficients of  $x^2$  by the symbols

$$\begin{aligned} E_1 &= (f - M_0)(f - M_1), \\ E_2 &= fM_1 - f^2 - 2M_0M_1, \\ E_3 &= M_0(f + M_1), \end{aligned} \quad (20)$$

it is easy to get the roots of Eq. (19),

$$\begin{aligned} x^2 &= \frac{-E_2 \pm \sqrt{E_2^2 - 4E_1E_3}}{2E_1} \\ &= \frac{-(fM_1 - f^2 - 2M_0M_1) \pm (f^2 - fM_1 - 2fM_0)}{2(f - M_0)(f - M_1)}. \end{aligned} \quad (21)$$

By retaining the “+” sign in Eq. (21), we get  $x^2 = 1$ , which is obviously a trivial root and should be discarded. However, if the “−” sign is adopted, we obtain the physically meaningful root as

$$\begin{aligned} x^2 &= \frac{M_0(f + M_1)}{(f - M_0)(f - M_1)} \\ &= \frac{(D_2 + D_1) - (D_2 - D_1)f}{(D_2 + D_1) + (D_2 - D_1)f} \frac{B_2}{B_2 + (B_1 - B_2)f}. \end{aligned} \quad (22)$$

By applying the definition of  $x$  and recognizing the sound velocity in the fluid matrix as

$$V_1 = \sqrt{\frac{B_1}{D_1}}, \quad (23)$$

we arrive at the effective sound velocity of the composite,

$$V_{eff} = \sqrt{\frac{B_{eff}}{D_{eff}}} = \sqrt{\frac{\frac{B_2}{B_2 + (B_1 - B_2)f} B_1}{\frac{(D_2 + D_1) + (D_2 - D_1)f}{(D_2 + D_1) - (D_2 - D_1)f} D_1}}. \quad (24)$$

It is well known that according to the effective medium theory (EMT),<sup>11</sup> the effective bulk modulus  $B_{eff}$  of the fluid-solid composite is given by

$$\frac{1}{B_{eff}} = \frac{1-f}{B_1} + \frac{f}{B_2} \quad (25a)$$

or

$$B_{eff} = \frac{B_2}{B_2 + (B_1 - B_2)f} B_1. \quad (25b)$$

It can be seen from Eqs. (17), (25a), and (25b) that the effective bulk modulus  $B_{eff}$  is completely determined by the  $n=0$  angular scattering channel.

By using Eq. (24) and the effective medium expressions for  $B_{eff}$  [i.e., Eqs. (25a) and (25b)], we arrive precisely at the Berryman effective mass density in two dimensions,

$$\frac{D_{eff} - D_1}{D_{eff} + D_1} = f \frac{D_2 - D_1}{D_2 + D_1} \quad (26a)$$

or

$$D_{eff} = \frac{(D_2 + D_1) + (D_2 - D_1)f}{(D_2 + D_1) - (D_2 - D_1)f} D_1. \quad (26b)$$

At this point it is interesting to note that the effective mass density  $D_{eff}$  is completely determined by the  $n=1$  angular channel. As pointed out previously, the effective mass density and the effective bulk modulus represent separate but parallel wave scattering channels.

Equation (24) is noted to be valid for both the square and the hexagonal lattices to  $\omega^{-2}$ . That is, the effective wave speed is indeed independent of the microstructure to the leading order, as mentioned previously. Hence, the effective mass density expression is generally valid for isotropic composites. Our derivation also verifies at the same time the effective bulk modulus formulas [Eqs. (25a) and (25b)], which are valid in general for isotropic composites consisting of solid inclusions in fluid.<sup>11</sup>

However, when the concentration of scatterers is very high (near close packing), it is expected that higher-order terms in  $T^{-1}$  and  $G$  matrices would no longer be negligible. It is physically understandable that the dipole approximation is not accurate enough to describe the situation where the scatterers almost touch each other. For such high concentrations, the effective sound speeds can be different for the square and the hexagonal lattices, although isotropy still holds.

### C. Solid-matrix composites

If the matrix is made of solid instead of liquid, we can also take its low-frequency limit in a similar way. However, a different effective medium formula may be expected since in the solid matrix not only longitudinal waves but also transverse waves can propagate. It is well known that in two-dimensional phononic crystals, when the wave vector is confined in the 2D plane (i.e., the  $x$ - $y$  plane) perpendicular to the cylinder axis direction (i.e., the  $z$  direction), the elastic waves can be decoupled into an out-of-plane transverse  $z$  mode and an in-plane mixed  $xy$  mode.<sup>12</sup>

As shown schematically in Fig. 2, for the transverse  $z$  mode the displacement is always perpendicular to the  $x$ - $y$  plane, and thus easier to deal with. By taking the low-frequency limit on the rigorous MST<sup>12</sup> and retaining the dominant terms, the  $T^{-1} - G$  matrix can also be simplified to a  $3 \times 3$  matrix (see Appendix C for details),

$$T^{-1} - G = \frac{4i}{\pi r^2} \frac{1}{\beta_1^2} \begin{bmatrix} \frac{\mu_2 + \mu_1}{\mu_2 - \mu_1} + f \frac{x^2}{1-x^2} & \frac{ixf}{1-x^2} e^{-i\theta_0} & -\frac{f}{1-x^2} e^{-2i\theta_0} \\ -\frac{ixf}{1-x^2} e^{i\theta_0} & \frac{D_1}{D_1 - D_2} + f \frac{x^2}{1-x^2} & \frac{ixf}{1-x^2} e^{-i\theta_0} \\ -\frac{f}{1-x^2} e^{2i\theta_0} & -\frac{ixf}{1-x^2} e^{i\theta_0} & \frac{\mu_2 + \mu_1}{\mu_2 - \mu_1} + f \frac{x^2}{1-x^2} \end{bmatrix}, \quad (27)$$

in which  $x = V_{eff}/V_1$  is the quantity to be evaluated. By defining the dimensionless quantities  $M'_0$  and  $M'_1$  as

$$M'_0 = \frac{D_1}{D_1 - D_2},$$

$$M'_1 = \frac{\mu_2 + \mu_1}{\mu_2 - \mu_1}, \quad (28)$$

the secular equation  $\det|T^{-1} - G| = 0$  can be written as

$$(f - M'_0)(f - M'_1)x^4 + (fM'_1 - f^2 - 2M'_0M'_1)x^2 + M'_0(f + M'_1) = 0. \quad (29)$$

By solving Eq. (29), we obtain the root

$$x^2 = \frac{M'_0(f + M'_1)}{(f - M'_0)(f - M'_1)} = \frac{D_1}{(1-f)D_1 + fD_2} \times \frac{(\mu_2 + \mu_1) + (\mu_2 - \mu_1)f}{(\mu_2 + \mu_1) - (\mu_2 - \mu_1)f}. \quad (30)$$

Since the definition of the transverse wave velocity in the solid matrix is given by

$$V_1 = \sqrt{\frac{\mu_1}{D_1}}, \quad (31)$$

we arrive at the effective transverse wave velocity of the composite as

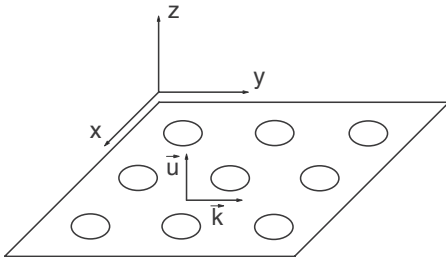


FIG. 2. The transverse  $z$  mode (i.e., the displacement vector is perpendicular to the  $x$ - $y$  plane) of the elastic waves propagating in a two-dimensional phononic crystal.

$$V_{eff} = \sqrt{\frac{\mu_{eff}}{D_{eff}}} = \sqrt{\frac{(\mu_2 + \mu_1) + (\mu_2 - \mu_1)f}{(\mu_2 + \mu_1) - (\mu_2 - \mu_1)f} \frac{\mu_1}{[(1-f)D_1 + fD_2]D_1}}. \quad (32)$$

It can be recognized from Eq. (32) that the effective shear modulus  $\mu_{eff}$ , completely determined by the  $n=1$  angular channel [see Eqs. (27) and below], is given by

$$\frac{\mu_{eff} - \mu_1}{\mu_{eff} + \mu_1} = f \frac{\mu_2 - \mu_1}{\mu_2 + \mu_1} \quad (33a)$$

or

$$\mu_{eff} = \frac{(\mu_2 + \mu_1) + (\mu_2 - \mu_1)f}{(\mu_2 + \mu_1) - (\mu_2 - \mu_1)f} \mu_1. \quad (33b)$$

Equations (33a) and (33b) are identical to that derived by Kuster and Toksöz<sup>1</sup> by using the averaged  $T$  matrix approximation. It is interesting to point out that Eqs. (33a) and (33b) have nearly the same form as Eqs. (26a) and (26b), and this similarity is due to the fact that both  $\mu_{eff}$  in Eqs. (33a) and (33b) and  $D_{eff}$  in Eqs. (26a) and (26b) arise from the  $n=1$  angular channel scattering.

According to Eq. (32) and the effective shear modulus expression for  $\mu_{eff}$ , i.e., Eqs. (33a) and (33b), we arrive at the VAMD for the transverse  $z$  mode,

$$D_{eff} = (1-f)D_1 + fD_2. \quad (34)$$

Distinct from the fluid-matrix case, here the effective mass density for the solid-matrix composite is determined by the  $n=0$  angular channel.

It should be noted that the volume-averaged mass density was found to be the quantity in predicting the low-frequency wave velocity for the solid-matrix case by Berryman.<sup>2</sup> Here, we use the rigorous MST to verify this result.

If we let  $\mu_1 \rightarrow 0$ , then according to Eqs. (33a) and (33b) we have  $\mu_{eff} \rightarrow 0$ . That is, when the solid matrix is gradually reduced to the limit of zero shear modulus, then the whole composite would also act like a zero shear modulus system; i.e., the composite would behave like a fluid. However, it is important to note that even in this limit the VAMD formula, i.e., Eq. (34), still holds. That is, the order of taking the two limits *cannot* be interchanged. By first taking the low-frequency  $\omega \rightarrow 0$  limit and then the  $\mu_1 \rightarrow 0$  limit, we arrive at the VAMD expression. However, reversing the order of taking the two limits leads to the expressions given by Eqs. (26a) and (26b). The physical reason for this noninterchangeability will become clear in the following section.

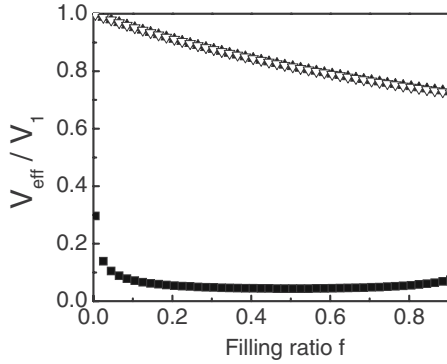


FIG. 3. The effective sound velocities calculated with the effective bulk modulus given by Eqs. (25a) and (25b) with VAMD (solid squares), and with the mass density given by Eqs. (26a) and (26b) (solid triangle). The experimentally measured effective sound velocity is shown as open triangles. While the VAMD gives results very far removed from the experiment, the mass density given by Eqs. (26a) and (26b) is shown to yield an almost perfect agreement with measured results.

#### V. COMPARISON WITH EXPERIMENTAL DATA

Cervera *et al.* have recently measured the sound velocity in a two-dimensional phononic crystal composed of a hexagonal array of aluminum cylinders in air.<sup>7</sup> Here, the frequency of sound is 600 Hz and the Al cylinders have a maximum diameter of 3.175 cm, with a hexagonal lattice constant of 6.35 cm. The wavelength of sound in air, 57 cm, is thus much larger than either the cylinder diameter or the lattice constant. The wavelengths of sound in Al, 10.68 m for the longitudinal wave and 5.19 m for the transverse wave, are even larger. The use of the effective medium prediction is thus justified. The viscosity and mass density of air at normal temperature are  $1.827 \times 10^{-5}$  Pa s and  $1.292 \text{ kg/m}^3$ , respectively. The minimum cylinder-cylinder (surface to surface) separation is 2.35 cm. At the experimental frequency of  $\sim 600$  Hz, we have  $\eta/\rho\omega l^2 \ll 1$ . Thus, the boundary condition of the zero tangential shear stress is justified. In Fig. 3, it is seen that there is a very large discrepancy between the experimentally measured velocity with that predicted by using the VAMD and the effective bulk modulus  $B_{eff}$  given by Eqs. (25a) and (25b). In contrast, when the dynamic effective mass density given by Eqs. (26a) and (26b) is used, an excellent agreement is seen. The difference between the two predictions lies in the fact that the VAMD is an upper bound to the dynamic mass density [Eqs. (26a) and (26b)]. This can be easily seen by subtracting the two expressions,

$$\begin{aligned} \rho_{eff} - D_{eff} &= [(1-f)D_1 + fD_2] - \frac{(D_2 + D_1) + (D_2 - D_1)f}{(D_2 + D_1) - (D_2 - D_1)f} \\ &= \frac{f(1-f)(D_1 - D_2)^2}{D_1(1+f) + D_2(1-f)} \geq 0. \end{aligned}$$

As the static version of the effective mass density must be the VAMD (verifiable through a simple weighing of the composite and its constituents and by measuring the volumes), the reason for the different (long wavelength) dynamic ver-

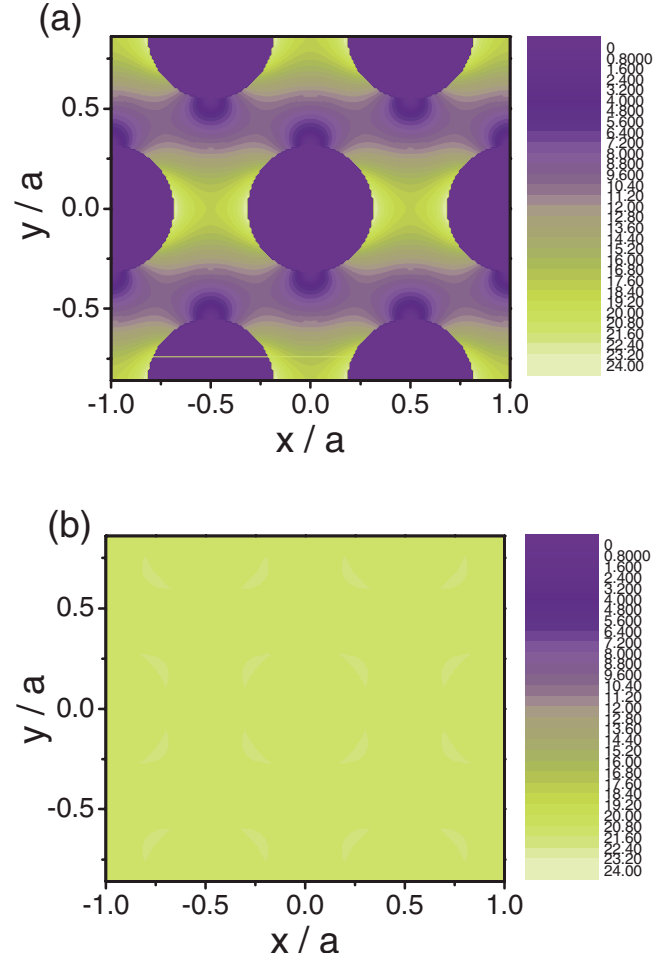


FIG. 4. (Color online) (a) MST-calculated displacement field intensities in a 2D hexagonal lattice of Al cylinders in air, with the relevant experimental parameter values as those in Ref. 7. Blue (dark gray) indicates low field intensity, and yellow (light gray) indicates high field intensity. The wave vector is along the  $y$  direction, with  $a$  being the lattice constant. It is seen that the wave amplitude is nearly zero inside the Al cylinders. Decreasing the frequency further does not alter this fact. (b) The same for PMMA cylinders in water. The wave field is seen to be much more homogeneous than that in (a).

sion can be found in the fact that for wave properties, VAMD contains the implicit assumption of wave field homogeneity in the long wavelength limit. This assumption can be violated (even in the long wavelength limit) when there is a very large impedance mismatch between the two components, such as in the experiment of Cervera *et al.* In Fig. 4(a), we show the numerically calculated wave field intensities (using MST), in color, for the relevant experiment. It is noted that the wave field is nearly zero inside the cylinders, which is plausible. Hence, it is almost impossible to have the condition for the validity of VAMD, and the observed decrease in wave velocity with increasing solid cylinder concentration can be ascribed to the increased wave paths' tortuosity. However, when the impedance mismatch is relatively moderate, e.g., when the mass density contrast is small, then the effective dynamic mass density yields the VAMD. That is, VAMD

can be a special case of the dynamic mass density. For comparison with Fig. 4(a), we have also plotted the displacement field intensities for the polymethyl methacrylate (PMMA)-water system in Fig. 4(b), in which the wave field homogeneity is very evident. As our derivation is obtained by taking the long wavelength limit of the scattering wave field solutions, it is not surprising that such formula inherently accounts for the wave field inhomogeneities as they exist in reality. We may conclude that *relative motion* between the components of a composite is the basic reason leading to the difference between the VAMD and the effective dynamic mass density.

It follows that in a solid-matrix composite, the presence of a finite shear modulus for the matrix component means that in the long wavelength limit, the uniform motion of the matrix and the inclusions is guaranteed. As a result, the dynamic mass density for the solid-matrix composites is always the VAMD. When one further takes the limit of  $\mu_1 \rightarrow 0$  in that case, only the relative ratio of the longitudinal wavelength to the transverse (shear) wavelength is altered, which is the reason that the effective mass density expression still remains the same as VAMD.

## VI. EFFECTIVE MASS DENSITY AT FINITE FREQUENCIES

The underlying physical reason for the existence of two mass densities, i.e., the relative motion between the constituents of a composite, implies that if there are local resonances (e.g., arising from the microstructure and material properties of the inclusions), some very interesting behaviors can result. In this section, we extend the effective dynamic mass density expressions, [Eqs. (26a) and (26b)] to finite frequencies. By employing the CPA,<sup>11</sup> we show that a generalized effective mass density expression can be obtained, which reduces to Eqs. (26a) and (26b) in the long wavelength limit and which can yield complex and negative dynamic mass densities when there exist low-frequency resonances. While the CPA was originally developed for the long wavelength limit (or the low-frequency limit), here the extension to finite frequencies is based on the idea that we can treat the case of matrix plus inclusions by requiring only the wavelength in the matrix to be much larger than the size of the inclusions or the inclusion separations. The inclusion is treated as a black-box scatterer, in which there can be complex fine-scale internal microstructures, with material properties such that the usual CPA requirement of long wavelength (compared to the typical feature size) can be violated. So, the scattering from the inclusion(s) will be represented by the accurately evaluated (either numerically or analytically) scattering amplitude(s). The scattering from the inclusion can even include local resonances internal to the inclusions. Such extension to the finite frequency regime is sometimes denoted as the dynamical CPA (DCPA), or dynamical EMT.<sup>13</sup> Below, we first treat the fluid-matrix case, followed by the solid-matrix case.

### A. Fluid-matrix composites

Consider a composite consisting of solid particle inclusions with mass density  $D_2$  and Lamé constants  $\lambda_2$  and  $\mu_2$

(assuming the inclusions have no fine-scale microstructure) embedded in a fluid matrix with mass density  $D_1$  and Lamé constant  $\lambda_1$ . In accordance with the rule of CPA, we assume that the parameters for the effective medium are  $D_{eff}$  and  $\lambda_{eff}$ , which are to be determined by minimizing the average overall scattering of the system. Accordingly, the wave numbers in the fluid, the particle, and the effective medium are  $\alpha_1$ ,  $\alpha_2$ , and  $\alpha_{eff}$ , respectively.

To illustrate the geometry of the CPA calculation, we show in Fig. 5 the basic idea of homogenization. That is, in Fig. 5(a) the dashed lines schematically divide the composite into similar structural units, each consisting of an inclusion with a layer of the matrix material. For the purpose of CPA calculation, the composite in Fig. 5(a) is replaced by the geometry shown in Fig. 5(b), in which the medium outside of one particular structural unit is treated as a homogeneous effective medium, whereby the origin is set at the center and the area of the structural unit (consisting of the inclusion and the matrix coating layer) of radius  $R$  is defined to be the same as the area of one unit cell, while the radius of the core (the inclusion) is given by  $r$ . The idea here is that the effective medium is composed of similar structural units (see Ref. 11). The cylindrical inclusion may have finer-scale internal microstructures that are not detailed at this level.

Within the layer of the fluid medium, the displacement field can be written as

$$\vec{u}_1(\vec{\rho}) = \sum_n \{a_n(1) \nabla [J_n(\alpha_1 \rho) e^{in\varphi}] + b_n(1) \nabla [H_n(\alpha_1 \rho) e^{in\varphi}]\}, \quad (35)$$

in which  $a_n(1)$  and  $b_n(1)$  have the relationship

$$b_n(1) = S_n(1)a_n(1), \quad (36)$$

where  $S_n(1) = T_{nn}$  is exactly the Mie scattering coefficient defined in Eq. (11).

The displacement field in the effective medium can be written similarly as

$$\vec{u}_{eff}(\vec{\rho}) = \sum_n \{a_n(\text{eff}) \nabla [J_n(\alpha_{eff} \rho) e^{in\varphi}] + b_n(\text{eff}) \nabla [H_n(\alpha_{eff} \rho) e^{in\varphi}]\}, \quad (37)$$

in which  $a_n(\text{eff})$  and  $b_n(\text{eff})$  are related by  $S_n(\text{tot})$  as

$$b_n(\text{eff}) = S_n(\text{tot})a_n(\text{eff}), \quad (38)$$

where  $S_n(\text{tot})$  is the scattering cross section for the whole coated particle.

By matching the normal components of displacement and pressure on the interface between the fluid medium and the effective medium, we get the following equations:

$$\begin{aligned} & \left[ \frac{dJ_n(\alpha_{eff}\rho)}{d\rho} \right]_{\rho=R} a_n(\text{eff}) + \left[ \frac{dH_n(\alpha_{eff}\rho)}{d\rho} \right]_{\rho=R} b_n(\text{eff}) \\ & = \left[ \frac{dJ_n(\alpha_1\rho)}{d\rho} \right]_{\rho=R} a_n(1) + \left[ \frac{dH_n(\alpha_1\rho)}{d\rho} \right]_{\rho=R} b_n(1), \quad (39) \end{aligned}$$

$$\begin{aligned}
& \lambda_{eff} \left[ \frac{dJ_n(\alpha_{eff}\rho)}{d\rho} + \rho \frac{d^2J_n(\alpha_{eff}\rho)}{d\rho^2} - \frac{n^2J_n(\alpha_{eff}\rho)}{\rho} \right]_{\rho=R} a_n(\text{eff}) \\
& + \lambda_{eff} \left[ \frac{dH_n(\alpha_{eff}\rho)}{d\rho} + \rho \frac{d^2H_n(\alpha_{eff}\rho)}{d\rho^2} \right. \\
& \quad \left. - \frac{n^2H_n(\alpha_{eff}\rho)}{\rho} \right]_{\rho=R} b_n(\text{eff}) \\
& = \lambda_1 \left[ \frac{dJ_n(\alpha_1\rho)}{d\rho} + \rho \frac{d^2J_n(\alpha_1\rho)}{d\rho^2} - \frac{n^2J_n(\alpha_1\rho)}{\rho} \right]_{\rho=R} a_n(1) \\
& + \lambda_1 \left[ \frac{dH_n(\alpha_1\rho)}{d\rho} + \rho \frac{d^2H_n(\alpha_1\rho)}{d\rho^2} - \frac{n^2H_n(\alpha_1\rho)}{\rho} \right]_{\rho=R} b_n(1).
\end{aligned} \tag{40}$$

In the lowest order of frequency, the scattering cross section is dominated by the  $n=0$  and  $n=\pm 1$  terms only. In order to minimize the overall average scattering of the system, CPA requires the lowest orders of scattering coefficients to be zero, i.e.,

$$S_n(\text{tot}) = 0 \tag{41}$$

for  $n=0, \pm 1$ . This condition is physically sensible since only then can one treat the medium as being a homogeneous effective medium in some sense. After substituting Eqs. (36) and (38)–(40) into Eq. (41), we get

$$\begin{aligned}
& \frac{nJ_n(\alpha_1R) - \alpha_1RJ_{n+1}(\alpha_1R)}{nJ_n(\alpha_{eff}R) - \alpha_{eff}RJ_{n+1}(\alpha_{eff}R)} \\
& - \frac{\lambda_1}{\lambda_{eff}} \frac{-2(n+1)\alpha_1RJ_{n+1}(\alpha_1R) + (\alpha_1R)^2J_{n+2}(\alpha_1R)}{-2(n+1)\alpha_{eff}RJ_{n+1}(\alpha_{eff}R) + (\alpha_{eff}R)^2J_{n+2}(\alpha_{eff}R)} \\
& = \left[ \frac{\lambda_1}{\lambda_{eff}} \frac{-2(n+1)\alpha_1RH_{n+1}(\alpha_1R) + (\alpha_1R)^2H_{n+2}(\alpha_1R)}{-2(n+1)\alpha_{eff}RJ_{n+1}(\alpha_{eff}R) + (\alpha_{eff}R)^2J_{n+2}(\alpha_{eff}R)} \right. \\
& \quad \left. - \frac{nH_n(\alpha_1R) - \alpha_1RH_{n+1}(\alpha_1R)}{nJ_n(\alpha_{eff}R) - \alpha_{eff}RJ_{n+1}(\alpha_{eff}R)} \right] S_n(1).
\end{aligned} \tag{42}$$

By retaining the dominant terms to the order of  $\omega^2$  in the series expansions of Bessel and Hankel functions, we arrive at the following formulas

$$-1 + \frac{\lambda_1}{\lambda_{eff}} = \frac{4}{i\pi(\alpha_1R)^2} S_0(1), \tag{43}$$

$$\frac{D_{eff} - D_1}{D_{eff} + D_1} = \frac{4}{i\pi(\alpha_1R)^2} S_1(1), \tag{44}$$

where  $S_n(1)=T_{nn}$  is the Mie scattering coefficient as defined by Eq. (11). Alternatively, the equations may be written as

$$-1 + \frac{\lambda_1}{\lambda_{eff}} = \frac{4f}{i\pi(\alpha_1r)^2} S_0(1), \tag{45}$$

$$\frac{D_{eff} - D_1}{D_{eff} + D_1} = \frac{4f}{i\pi(\alpha_1r)^2} S_1(1), \tag{46}$$

in which  $f = \pi r^2 / \pi R^2 = (r/R)^2$  is the filling ratio of the solid cylinder, with  $r$  being the radius of the solid core.

In fact, as demonstrated in Appendix B, the Mie scattering coefficient  $T_{nn}$  has the following form:

$$S_n(1) = T_{nn} = \frac{(C_{21}C_{32} - C_{22}C_{31})A_1 - (C_{11}C_{32} - C_{12}C_{31})A_2}{(C_{11}C_{32} - C_{12}C_{31})B_2 - (C_{21}C_{32} - C_{22}C_{31})B_1}, \tag{47}$$

in which the coefficients  $A$ ,  $B$ , and  $C$  are defined in Eq. (B3). After some algebraic manipulation, it can be shown that

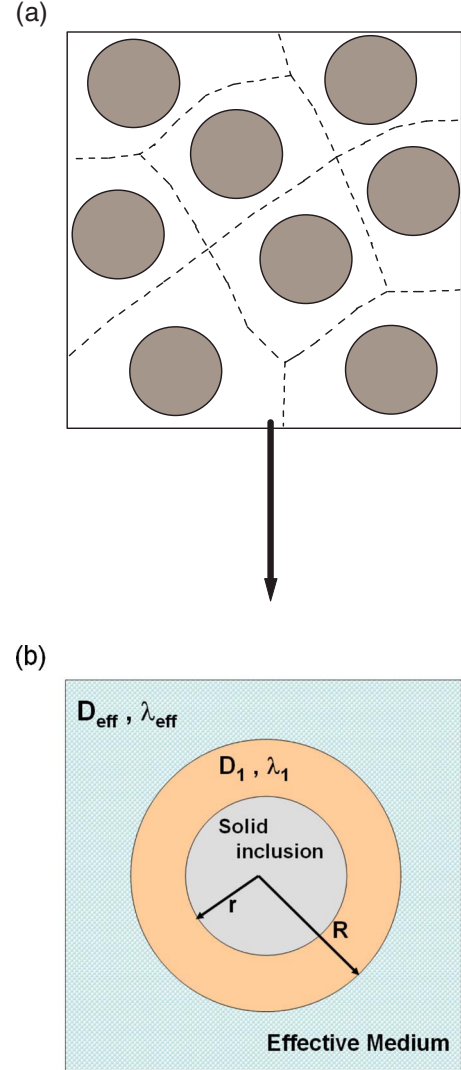


FIG. 5. (Color online) (a) Schematic diagram of the coherent potential approximation (CPA). The dashed lines indicate a schematic division of the composite into structure units, each consisting of an inclusion with a coating layer of the matrix material. (b) The composite in (a) is replaced by that represented in (b) for the CPA calculation, consisting of a coated cylinder of radius  $R$  embedded in the effective medium with parameters  $D_{eff}$  and  $\lambda_{eff}$ , to be determined by minimizing the overall average scattering. For the coated cylinder, the core is the inclusion and the coating is the matrix material.

$$S_1(1) = T_{11} = -\frac{F_1[J_1(\alpha_1 R) - \alpha_1 R J_2(\alpha_1 R)] + F_2[4J_2(\alpha_2 R) - \alpha_1 R J_3(\alpha_1 R)]}{F_1[H_1(\alpha_1 R) - \alpha_1 R H_2(\alpha_1 R)] + F_2[4H_2(\alpha_2 R) - \alpha_1 R H_3(\alpha_1 R)]}, \quad (48)$$

where  $F_1$  and  $F_2$  are very complicated functions of variables  $\alpha_1$ ,  $\alpha_2$ ,  $\beta_2$ , and  $R$ . At this level,  $S_1(1)$  just denote the scattering amplitude from a single solid inclusion. Its accurate form (the  $F_1$  and  $F_2$ ) would depend on the internal microstructure and material properties of the solid inclusion unit. In the simplest case, it can be shown that if the core cylinder is made of a uniform solid medium, then by taking the low-frequency limit,  $S_1(1) \rightarrow [\pi(\alpha_1 r)^2/4i][(D_1 - D_2)/(D_1 + D_2)]$ ; i.e., one recovers Eqs. (26a) and (26b) exactly.

It should be noted that, as evident in Eq. (46), the effective mass density  $D_{eff}$  can be negative for  $|S_1(1)| > \pi(\alpha_1 r)^2/4f$ . However, if there is a resonance in the  $n=1$  channel, the modulus of the complex scattering amplitude can indeed be very large. This fact was noted in Ref. 14.

It is evident in Eq. (46) that the scattering coefficient is the basic reason for the complex and/or negative value of the effective mass density  $D_{eff}$ . To treat a more interesting case in which the solid inclusions can have fine-scale internal microstructures, let us regard each inclusion to consist of a lead cylinder coated by a layer of silicone rubber, i.e., the microstructure for the LRSM. This is shown schematically in Fig. 6. The numerically evaluated scattering coefficient  $S_1(1)$  (by using the MST) is plotted vs frequency in Fig. 7, together with the normalized effective mass density  $D_{eff}/D_1$ . The calculated system is that of a lead cylinder coated with a layer of silicone rubber, placed in water. The filling ratio of the coated cylinder (lead cylinder+silicone rubber coating) is 40%, while the filling ratio of just the lead cylinder is 25%. It can be seen from Fig. 7 that the complex or negative effective mass density of such type of locally resonant inclusions arises from the resonant behavior of the scattering coefficient. The mass density and elastic constants used in the calculation are as follows<sup>3</sup>  $\rho = 11.6 \times 10^3 \text{ kg/m}^3$ ,  $\lambda = 4.23 \times 10^{10} \text{ N/m}^2$ ,  $\mu = 1.49 \times 10^{10} \text{ N/m}^2$  for lead,  $\rho = 1.3 \times 10^3 \text{ kg/m}^3$ ,  $\lambda = 6 \times 10^5 \text{ N/m}^2$ ,  $\mu = 4 \times 10^4 \text{ N/m}^2$  for the silicone rubber, and  $\rho = 1.0 \times 10^3 \text{ kg/m}^3$ ,  $\lambda = 2.22 \times 10^9 \text{ N/m}^2$  for water. It is seen that first of all, there are two resonances, typical of the LRSM.<sup>4</sup> Also, the resonant behavior of the dynamic mass density occurs at frequencies different from those of the scattering coefficient. This is due to the fact that the divergence of the effective dynamic mass density occurs for those frequencies at which the right-hand side of Eq. (44) [or Eq. (46)] is 1.

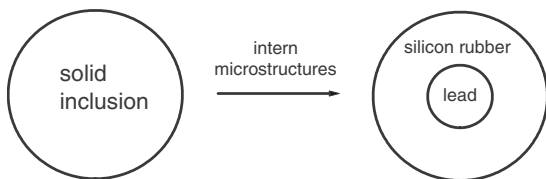


FIG. 6. An example of the locally resonant inclusion: Each inclusion can have a finer-scale microstructure, consisting of a lead cylinder coated by a layer of silicone rubber.

The physical picture about why the dynamic mass density can be negative should now be intuitively clear: It is caused by the  $180^\circ$  out-of-phase motion of the core lead cylinders. Since the core lead cylinder has a very high mass density and since the area fraction of such cylinders is sufficiently high, the net average result within a narrow frequency regime is that the overall effective dynamic mass density is negative. In this regard, complex dynamic mass density is just a generalization to the degree of phase lag between the displacement in the matrix and that of the lead cylinder motion.

Similarly, the finite frequency effective bulk modulus can also be numerically evaluated from Eq. (45). They are shown in Fig. 8. It is evident in Fig. 8 that the effective bulk modulus  $B_{eff}$  is very small in magnitude as compared to that of water. This is physically reasonable since the coated cylinders are very compressible (due to the soft coating), and when one mixes something hard with something soft, the compressibility (or bulk modulus) is dominated by the soft component, just as in the case of a sandwich made of two steel plates with a sponge in between, where the compressibility of the sandwich is clearly dominated by the sponge. On the high-frequency side, the real part of the effective bulk modulus also turns negative. However, we should not expect this to be the realization of acoustic metamaterials (as the effective dynamic mass density is also negative) since  $B_{eff}$  has a comparable imaginary component. When both are considered together, the phase and group velocities have the same direction.

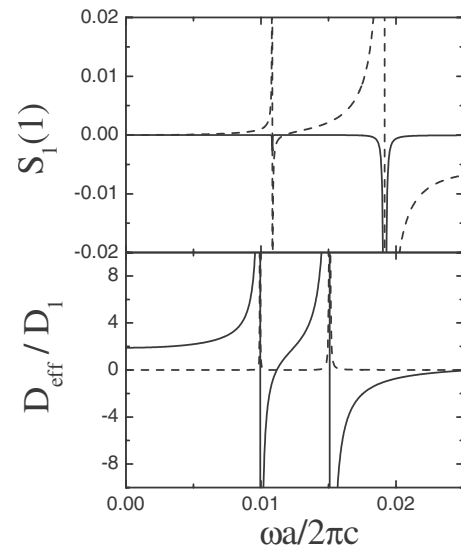


FIG. 7. The scattering coefficient  $S_1(1)$  and normalized effective mass density  $D_{eff}/D_1$  of a lead cylinder coated with a layer of silicone rubber, placed in water, as functions of normalized frequency  $\omega a/2\pi c$ , with  $c$  being the sound speed in water. The filling ratio of the coated cylinder is 40%, while the filling ratio of the lead cylinder is 25%. Solid lines and dashed lines denote the real and imaginary parts of the plotted quantities, respectively.

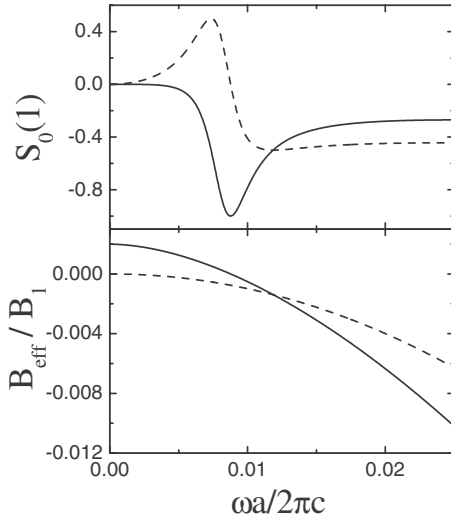


FIG. 8. The scattering coefficient  $S_0(1)$  and normalized effective bulk modulus  $B_{eff}/B_1$  of a lead cylinder coated with a layer of silicon rubber, placed in water, as functions of normalized frequency  $\omega a/2\pi c$ , with  $c$  being the sound speed in water. The filling ratio of the coated cylinder is 40%, while the filling ratio of the lead cylinder is 25%, i.e., the same structure unit as that in Fig. 7. Solid lines and dashed lines denote the real and imaginary parts of the plotted quantities, respectively.

### B. Solid-matrix composites

For the solid-matrix case, we can similarly extend the dynamic effective mass density expression to finite frequencies where there exist low-frequency resonances. We will show that for inclusions with a fine-scale microstructure that consists of a lead core and silicone rubber coating, the dynamic mass density can also be negative around resonances. This should not be surprising since in either the fluid-matrix case or the solid-matrix case the physical reason for the negative dynamic mass density is the out-of-phase motion of the core lead cylinder.

As in preceding sections, we assume that a solid cylinder, the inclusion, with mass density  $D_2$  and Lamé constants  $\lambda_2$  and  $\mu_2$  (assuming a uniform material with no fine-scale microstructure), is embedded in a matrix solid material with mass density  $D_1$  and Lamé constants  $\lambda_1$  and  $\mu_1$ . The geometry for the DCPA calculation is the same as that shown in Fig. 5; i.e., the inclusion plus a layer of matrix coating is embedded in the effective medium. We also assume that the parameters for the effective medium are  $D_{eff}$ ,  $\lambda_{eff}$  and  $\mu_{eff}$ , which are to be determined in accordance with the DCPA. Accordingly, the longitudinal and transverse wave numbers in the core, the coating layer, and the effective medium are  $\alpha_1$ ,  $\beta_1$ ,  $\alpha_2$ ,  $\beta_2$ , and  $\alpha_{eff}$ ,  $\beta_{eff}$ , respectively.

Similar to Fig. 5, the origin is set at the center of the core, and the area of the whole cylinder (including the core and coating layer) of radius  $R$  is defined to be the same as the area of one unit cell, while the radius of the core is  $r$ .

Within the coating layer, the displacement field can be written as.<sup>12</sup>

$$\begin{aligned} \vec{u}_1(\vec{\rho}) = & \sum_n \{a_{n1}(1) \nabla [J_n(\alpha_1 \rho) e^{in\varphi}] + b_{n1}(1) \nabla [H_n(\alpha_1 \rho) e^{in\varphi}]\} \\ & + \sum_n \{a_{n2}(1) \nabla \times [\hat{z} J_n(\beta_1 \rho) e^{in\varphi}] + b_{n2}(1) \nabla \\ & \times [\hat{z} H_n(\beta_1 \rho) e^{in\varphi}]\} \\ & + \sum_n \left\{ a_{n3}(1) \frac{1}{\beta_1} \nabla \times \nabla \times [\hat{z} J_n(\beta_1 \rho) e^{in\varphi}] \right. \\ & \left. + b_{n3}(1) \frac{1}{\beta_1} \nabla \times \nabla \times [\hat{z} H_n(\beta_1 \rho) e^{in\varphi}] \right\}, \end{aligned} \quad (49)$$

in which  $a_{n\sigma}(1)$  and  $b_{n\sigma}(1)$  have following relationship:

$$b_{n\sigma}(1) = \sum_{n'\sigma'} T_{n\sigma n'\sigma'}(1) a_{n'\sigma'}(1), \quad (50)$$

where  $\sigma=1$  is for the longitudinal mode and  $\sigma=2,3$  represents the two transverse modes, with  $T_{n\sigma n'\sigma'}(1)$  being the Mie scattering coefficients of the core.<sup>12</sup>

Similarly the displacement field in the effective medium can be written as

$$\begin{aligned} \vec{u}_{eff}(\vec{\rho}) = & \sum_n \{a_{n1}(eff) \nabla [J_n(\alpha_{eff} \rho) e^{in\varphi}] \\ & + b_{n1}(eff) \nabla [H_n(\alpha_{eff} \rho) e^{in\varphi}]\} + \sum_n \{a_{n2}(eff) \nabla \\ & \times [\hat{z} J_n(\beta_{eff} \rho) e^{in\varphi}] + b_{n2}(eff) \nabla \times [\hat{z} H_n(\beta_{eff} \rho) e^{in\varphi}]\} \\ & + \sum_n \left\{ a_{n3}(eff) \frac{1}{\beta_{eff}} \nabla \times \nabla \times [\hat{z} J_n(\beta_{eff} \rho) e^{in\varphi}] \right. \\ & \left. + b_{n3}(eff) \frac{1}{\beta_{eff}} \nabla \times \nabla \times [\hat{z} H_n(\beta_{eff} \rho) e^{in\varphi}] \right\}, \end{aligned} \quad (51)$$

in which  $a_n(eff)$  and  $b_n(eff)$  are related by

$$b_{n\sigma}(eff) = \sum_{n'\sigma'} T_{n\sigma n'\sigma'}(eff) a_{n'\sigma'}(eff), \quad (52)$$

in which  $T_{n\sigma n'\sigma'}(eff)$  is the Mie scattering coefficients for the whole coated cylinder.

Displacement and normal stress continuity at the interface requires that

$$\begin{aligned} & \left[ \frac{dJ_n(\alpha_1 \rho)}{d\rho} \right]_{\rho=R} a_{n1}(1) + \left[ \frac{dH_n(\alpha_1 \rho)}{d\rho} \right]_{\rho=R} b_{n1}(1) \\ & + \left[ \frac{inJ_n(\beta_1 \rho)}{\rho} \right]_{\rho=R} a_{n2}(1) + \left[ \frac{inH_n(\beta_1 \rho)}{\rho} \right]_{\rho=R} b_{n2}(1) \\ = & \left[ \frac{dJ_n(\alpha_{eff} \rho)}{d\rho} \right]_{\rho=R} a_{n1}(eff) + \left[ \frac{dH_n(\alpha_{eff} \rho)}{d\rho} \right]_{\rho=R} b_{n1}(eff) \\ & + \left[ \frac{inJ_n(\beta_{eff} \rho)}{\rho} \right]_{\rho=R} a_{n2}(eff) + \left[ \frac{inH_n(\beta_{eff} \rho)}{\rho} \right]_{\rho=R} b_{n2}(eff), \end{aligned} \quad (53)$$

$$\begin{aligned}
& \left[ \frac{inJ_n(\alpha_1\rho)}{\rho} \right]_{\rho=R} a_{n1}(1) + \left[ \frac{inH_n(\alpha_1\rho)}{\rho} \right]_{\rho=R} b_{n1}(1) \\
& + \left[ \frac{-dJ_n(\beta_1\rho)}{d\rho} \right]_{\rho=R} a_{n2}(1) + \left[ \frac{-dH_n(\beta_1\rho)}{d\rho} \right]_{\rho=R} b_{n2}(1) \\
& = \left[ \frac{inJ_n(\alpha_{eff}\rho)}{\rho} \right]_{\rho=R} a_{n1}(\text{eff}) + \left[ \frac{inH_n(\alpha_{eff}\rho)}{\rho} \right]_{\rho=R} b_{n1}(\text{eff}) \\
& + \left[ \frac{-dJ_n(\beta_{eff}\rho)}{d\rho} \right]_{\rho=R} a_{n2}(\text{eff}) \\
& + \left[ \frac{-dH_n(\beta_{eff}\rho)}{d\rho} \right]_{\rho=R} b_{n2}(\text{eff}), \tag{54}
\end{aligned}$$

$$\begin{aligned}
& \left[ \frac{(2n+2)J_{n+1}(\beta_1\rho) - \beta_1\rho J_{n+2}(\beta_1\rho)}{\rho} \right]_{\rho=R} a_{n3}(1) \\
& + \left[ \frac{(2n+2)H_{n+1}(\beta_1\rho) - \beta_1\rho H_{n+2}(\beta_1\rho)}{\rho} \right]_{\rho=R} b_{n3}(1) \\
& = \left[ \frac{(2n+2)J_{n+1}(\beta_{eff}\rho) - \beta_{eff}\rho J_{n+2}(\beta_{eff}\rho)}{\rho} \right]_{\rho=R} a_{n3}(\text{eff}) \\
& + \left[ \frac{(2n+2)H_{n+1}(\beta_{eff}\rho) - \beta_{eff}\rho H_{n+2}(\beta_{eff}\rho)}{\rho} \right]_{\rho=R} b_{n3}(\text{eff}), \tag{55}
\end{aligned}$$

---


$$\begin{aligned}
& \left[ \frac{2\mu_1(n^2-n)J_n(\alpha_1\rho) - [\lambda_1(2n+2) + 2\mu_1(2n+1)]\alpha_1\rho J_{n+1}(\alpha_1\rho) + (\lambda_1 + 2\mu_1)\alpha_1^2\rho^2 J_{n+2}(\alpha_1\rho)}{\rho} \right]_{\rho=R} a_{n1}(1) \\
& + \left[ \frac{2\mu_1(n^2-n)H_n(\alpha_1\rho) - [\lambda_1(2n+2) + 2\mu_1(2n+1)]\alpha_1\rho H_{n+1}(\alpha_1\rho) + (\lambda_1 + 2\mu_1)\alpha_1^2\rho^2 H_{n+2}(\alpha_1\rho)}{\rho} \right]_{\rho=R} b_{n1}(1) \\
& + \left[ 2in\mu_1 \frac{(n-1)J_n(\beta_1\rho) - \beta_1\rho J_{n+1}(\beta_1\rho)}{\rho} \right]_{\rho=R} a_{n2}(1) + \left[ 2in\mu_1 \frac{(n-1)H_n(\beta_1\rho) - \beta_1\rho H_{n+1}(\beta_1\rho)}{\rho} \right]_{\rho=R} b_{n2}(1) \\
& = \left[ \frac{2\mu_{eff}(n^2-n)J_n(\alpha_{eff}\rho) - [\lambda_{eff}(2n+2) + 2\mu_{eff}(2n+1)]\alpha_{eff}\rho J_{n+1}(\alpha_{eff}\rho) + (\lambda_{eff} + 2\mu_{eff})\alpha_{eff}^2\rho^2 J_{n+2}(\alpha_{eff}\rho)}{\rho} \right]_{\rho=R} a_{n1}(\text{eff}) \\
& + \left[ \frac{2\mu_{eff}(n^2-n)H_n(\alpha_{eff}\rho) - [\lambda_{eff}(2n+2) + 2\mu_{eff}(2n+1)]\alpha_{eff}\rho H_{n+1}(\alpha_{eff}\rho) + (\lambda_{eff} + 2\mu_{eff})\alpha_{eff}^2\rho^2 H_{n+2}(\alpha_{eff}\rho)}{\rho} \right]_{\rho=R} b_{n1}(\text{eff}) \\
& + \left[ 2in\mu_{eff} \frac{(n-1)J_n(\beta_{eff}\rho) - \beta_{eff}\rho J_{n+1}(\beta_{eff}\rho)}{\rho} \right]_{\rho=R} a_{n2}(\text{eff}) + \left[ 2in\mu_{eff} \frac{(n-1)H_n(\beta_{eff}\rho) - \beta_{eff}\rho H_{n+1}(\beta_{eff}\rho)}{\rho} \right]_{\rho=R} b_{n2}(\text{eff}), \tag{56}
\end{aligned}$$

$$\begin{aligned}
& \left[ 2in\mu_1 \frac{(n-1)J_n(\alpha_1\rho) - \alpha_1\rho J_{n+1}(\alpha_1\rho)}{\rho} \right]_{\rho=R} a_{n1}(1) + \left[ 2in\mu_1 \frac{(n-1)H_n(\alpha_1\rho) - \alpha_1\rho H_{n+1}(\alpha_1\rho)}{\rho} \right]_{\rho=R} b_{n1}(1) \\
& + \left[ \mu_1 \frac{2(n-n^2)J_n(\beta_1\rho) + 2n\beta_1\rho J_{n+1}(\beta_1\rho) - \beta_1^2\rho^2 J_{n+2}(\beta_1\rho)}{\rho} \right]_{\rho=R} a_{n2}(1) \\
& + \left[ \mu_1 \frac{2(n-n^2)H_n(\beta_1\rho) + 2n\beta_1\rho H_{n+1}(\beta_1\rho) - \beta_1^2\rho^2 H_{n+2}(\beta_1\rho)}{\rho} \right]_{\rho=R} b_{n2}(1) \\
& = \left[ 2in\mu_{eff} \frac{(n-1)J_n(\alpha_{eff}\rho) - \alpha_{eff}\rho J_{n+1}(\alpha_{eff}\rho)}{\rho} \right]_{\rho=R} a_{n1}(\text{eff}) + \left[ 2in\mu_{eff} \frac{(n-1)H_n(\alpha_{eff}\rho) - \alpha_{eff}\rho H_{n+1}(\alpha_{eff}\rho)}{\rho} \right]_{\rho=R} b_{n1}(\text{eff}) \\
& + \left[ \mu_{eff} \frac{2(n-n^2)J_n(\beta_{eff}\rho) + 2n\beta_{eff}\rho J_{n+1}(\beta_{eff}\rho) - \beta_{eff}^2\rho^2 J_{n+2}(\beta_{eff}\rho)}{\rho} \right]_{\rho=R} a_{n2}(\text{eff}) \\
& + \left[ \mu_{eff} \frac{2(n-n^2)H_n(\beta_{eff}\rho) + 2n\beta_{eff}\rho H_{n+1}(\beta_{eff}\rho) - \beta_{eff}^2\rho^2 H_{n+2}(\beta_{eff}\rho)}{\rho} \right]_{\rho=R} b_{n2}(\text{eff}), \tag{57}
\end{aligned}$$

$$\begin{aligned}
& \left[ \mu_1 \frac{2n(n+1)J_{n+1}(\beta_1\rho) - (3n+4)\beta_1\rho J_{n+2}(\beta_1\rho) + \beta_1^2\rho^2 J_{n+3}(\beta_1\rho)}{\rho} \right]_{\rho=R} a_{n3}(1) \\
& + \left[ \mu_1 \frac{2n(n+1)H_{n+1}(\beta_1\rho) - (3n+4)\beta_1\rho H_{n+2}(\beta_1\rho) + \beta_1^2\rho^2 H_{n+3}(\beta_1\rho)}{\rho} \right]_{\rho=R} b_{n3}(1) \\
& = \left[ \mu_{eff} \frac{2n(n+1)J_{n+1}(\beta_{eff}\rho) - (3n+4)\beta_{eff}\rho J_{n+2}(\beta_{eff}\rho) + \beta_{eff}^2\rho^2 J_{n+3}(\beta_{eff}\rho)}{\rho} \right]_{\rho=R} a_{n3}(eff) \\
& + \left[ \mu_{eff} \frac{2n(n+1)H_{n+1}(\beta_{eff}\rho) - (3n+4)\beta_{eff}\rho H_{n+2}(\beta_{eff}\rho) + \beta_{eff}^2\rho^2 H_{n+3}(\beta_{eff}\rho)}{\rho} \right]_{\rho=R} b_{n3}(eff). \quad (58)
\end{aligned}$$

In the lowest order of frequency, the scattering cross section is dominated by the  $n=0$  and  $n=\pm 1$  terms only. The rule of the DCPA is to require the lowest orders of Mie scattering coefficients to be zero,

$$T_{n\sigma n'\sigma'}(eff)|_{n,n'=\pm 1} = 0. \quad (59)$$

After substituting Eqs. (50) and (52)–(58) into Eq. (59) and retaining the dominant terms to the order of  $\omega^2$  in the series expansions of Bessel and Hankel functions, we arrive at the following formulas:

$$\frac{D_{eff}}{D_1} - 1 = \frac{4}{i\pi(\beta_1 R)^2} \frac{b_{03}(1)}{a_{03}(1)}, \quad (60)$$

$$\frac{\mu_{eff} - \mu_1}{\mu_{eff} + \mu_1} = \frac{4i}{\pi(\beta_1 R)^2} \frac{b_{13}(1)}{a_{13}(1)}, \quad (61)$$

$$\frac{(\lambda_{eff} + \mu_{eff}) - (\lambda_1 + \mu_1)}{\lambda_{eff} + \mu_{eff} + \mu_1} = \frac{4i}{\pi(\alpha_1 R)^2} \frac{b_{01}(1)}{a_{01}(1)}. \quad (62)$$

Alternatively, the above equations may be written as

$$\frac{D_{eff}}{D_1} - 1 = \frac{4f}{i\pi(\beta_1 r)^2} \frac{b_{03}(1)}{a_{03}(1)}, \quad (63)$$

$$\frac{\mu_{eff} - \mu_1}{\mu_{eff} + \mu_1} = \frac{4if}{\pi(\beta_1 r)^2} \frac{b_{13}(1)}{a_{13}(1)}, \quad (64)$$

$$\frac{(\lambda_{eff} + \mu_{eff}) - (\lambda_1 + \mu_1)}{\lambda_{eff} + \mu_{eff} + \mu_1} = \frac{4if}{\pi(\alpha_1 r)^2} \frac{b_{01}(1)}{a_{01}(1)}, \quad (65)$$

in which  $f = \pi r^2 / \pi R^2 = (r/R)^2$  is the filling ratio of the solid cylinder, with  $r$  being the radius of the solid core.

Since  $b_{03}(1)/a_{03}(1)$  is the  $n=0$  channel scattering coefficient for the  $z$ -direction transverse mode in the solid matrix, it is a complex number in general. As evident from Eq. (63), the real part of the dynamic effective mass density  $D_{eff}$  can be negative for  $\text{Im}[b_{03}(1)/a_{03}(1)] < -\pi(\beta_1 r)^2/4f$ . However, if there is a resonance in the  $n=0$  channel, the imaginary part of the complex scattering amplitude can be a very large negative number, so the effective mass density can turn negative as well.

If the inclusions have no fine-scale microstructure and consist of uniform materials, then in the low-frequency limit,

$$\frac{b_{03}(1)}{a_{03}(1)} \rightarrow \frac{i\pi(\beta_1 r)^2}{4} \left[ \frac{D_2}{D_1} - 1 \right],$$

$$\frac{b_{13}(1)}{a_{13}(1)} \rightarrow \frac{\pi(\beta_1 r)^2}{4i} \left[ \frac{\mu_2 - \mu_1}{\mu_2 + \mu_1} \right],$$

$$\frac{b_{01}(1)}{a_{01}(1)} \rightarrow \frac{\pi(\alpha_1 r)^2}{4i} \left[ \frac{(\lambda_2 + \mu_2) - (\lambda_1 + \mu_1)}{\lambda_2 + \mu_2 + \mu_1} \right].$$

Hence, the low-frequency limit of Eqs. (63)–(65) is given by

$$D_{eff} = (1-f)D_1 + fD_2, \quad (66)$$

$$\frac{\mu_{eff} - \mu_1}{\mu_{eff} + \mu_1} = f \frac{\mu_2 - \mu_1}{\mu_2 + \mu_1}, \quad (67)$$

$$\frac{(\lambda_{eff} + \mu_{eff}) - (\lambda_1 + \mu_1)}{\lambda_{eff} + \mu_{eff} + \mu_1} = f \frac{(\lambda_2 + \mu_2) - (\lambda_1 + \mu_1)}{\lambda_2 + \mu_2 + \mu_1}, \quad (68)$$

which are identical to Eqs. (34), (33a), and (33b). It is seen that the both the DCPA and the MST give the same effective medium formulas in the low-frequency limit, which is, of course, a physically consistent result.

In addition, Eq. (68) can also help us to determine  $\lambda_{eff}$  on the condition that  $\mu_{eff}$  is known. If we let  $\mu_1 \rightarrow 0$ , then according to Eq. (67), we have  $\mu_{eff} \rightarrow 0$ . It follows in that case that Eq. (68) reduces to

$$\frac{\lambda_{eff} - \lambda_1}{\lambda_{eff}} = f \frac{(\lambda_2 + \mu_2) - \lambda_1}{\lambda_2 + \mu_2}. \quad (69)$$

Since  $B_{eff} = \lambda_{eff}$ ,  $B_1 = \lambda_1$ , and  $B_2 = \lambda_2 + \mu_2$ , it is easy to realize that Eq. (69) is equivalent to

$$\frac{1}{B_{eff}} = \frac{1-f}{B_1} + \frac{f}{B_2}. \quad (70)$$

Not surprisingly, Eq. (70) is identical to Eqs. (25a) and (25b).

While the order for the two limit processes of  $\omega \rightarrow 0$  and  $\mu_1 \rightarrow 0$  can be interchanged for the effective moduli, the same is not true for the effective dynamic mass density as we noted earlier.

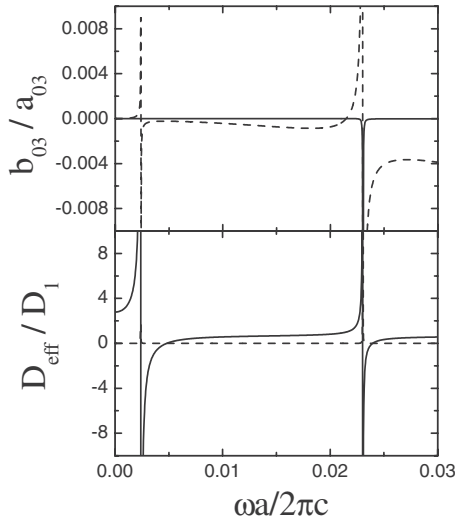


FIG. 9. The scattering coefficient  $b_{03}/a_{03}$  and normalized effective mass density  $D_{eff}/D_1$  of a lead cylinder coated with a layer of silicon rubber, placed in epoxy, as functions of normalized frequency  $\omega a/2\pi c$ , with  $c$  being the transverse velocity in epoxy. The filling ratio of the coated cylinder is 40%, while the filling ratio of the lead cylinder is 20%. Solid lines and dashed lines denote the real and imaginary parts of the plotted quantities, respectively.

If the inclusions have a fine-scale LRSM microstructure, just as that described in the previous section, i.e., a lead cylinder with a silicone rubber coating, then the scattering coefficient can be calculated numerically by using the MST. In Fig. 9, we show the scattering coefficient  $b_{03}/a_{03}$  and the normalized effective mass density  $D_{eff}/D_1$  plotted as functions of frequency (for a lead cylinder coated with a layer of silicone rubber, embedded in epoxy). The filling ratio of the coated cylinder is 40%, while the filling ratio of the lead cylinder is 20%. It is seen that the complex/negative effective mass density of such locally resonant structures corresponds exactly to the similar behavior of the scattering coefficient. While the parameters relevant to lead and silicone rubber are given previously, the parameters of epoxy are<sup>3</sup>  $\rho = 1.18 \times 10^3 \text{ kg/m}^3$ ,  $\lambda = 4.43 \times 10^9 \text{ N/m}^2$ , and  $\mu = 1.59 \times 10^9 \text{ N/m}^2$ .

From the plotted results, it can be seen that for locally resonant structures, it does not matter whether the matrix is fluid or solid. In both cases, a complex/negative effective dynamic mass density is obtained.

The finite frequency effective elastic moduli can be similarly evaluated by using the MST. The results are shown in Figs. 10 and 11. As evident in Eq. (64), the resonant behavior of the effective shear modulus in Fig. 10 corresponds exactly to the similar behavior of the scattering coefficient  $b_{13}/a_{13}$ . On the other hand, although no resonance exists in the curve of  $b_{01}/a_{01}$ , we still observe a resonant behavior in  $\lambda_{eff}/\lambda_1$ . The reason is that in Eq. (65),  $\lambda_{eff}$  and  $\mu_{eff}$  are coupled together: On the condition that the summation of them vary smoothly with frequency, the resonance of one will definitely lead to the resonance of the other.

## VII. RELEVANCE TO ACOUSTIC METAMATERIALS

We have shown through rigorous derivation that the effective dynamic mass density of an inhomogeneous mixture

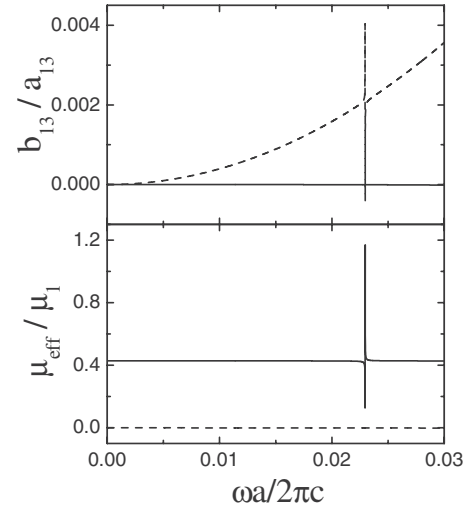


FIG. 10. The scattering coefficient  $b_{13}/a_{13}$  and normalized effective shear modulus  $\mu_{eff}/\mu_1$  of a lead cylinder coated with a layer of silicon rubber, placed in epoxy, as functions of normalized frequency  $\omega a/2\pi c$ , with  $c$  being the transverse velocity in epoxy. The filling ratio of the coated cylinder is 40%, while the filling ratio of the lead cylinder is 20%, i.e., the same structure unit as that in Fig. 9. Solid lines and dashed lines denote the real and imaginary parts of the plotted quantities, respectively.

can differ from its static counterpart even in the zero frequency limit (but must still be positive). The dynamic mass density can be negative or complex at finite frequencies when there are inclusions with locally resonant microstructures. These two results are shown to be consistent with each other and are related by the common underlying physics. The

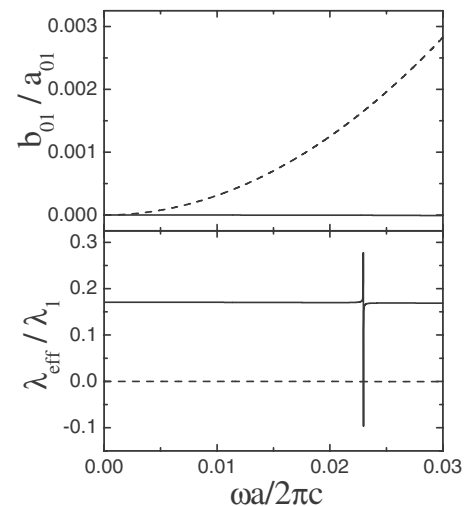


FIG. 11. The scattering coefficient  $b_{01}/a_{01}$  and normalized effective Lamé constant  $\lambda_{eff}/\lambda_1$  of a lead cylinder coated with a layer of silicon rubber, placed in epoxy, as functions of normalized frequency  $\omega a/2\pi c$ , with  $c$  being the transverse velocity in epoxy. The filling ratio of the coated cylinder is 40%, while the filling ratio of the lead cylinder is 20%, i.e., the same structure unit as that in Fig. 9. Solid lines and dashed lines denote the real and imaginary parts of the plotted quantities, respectively.

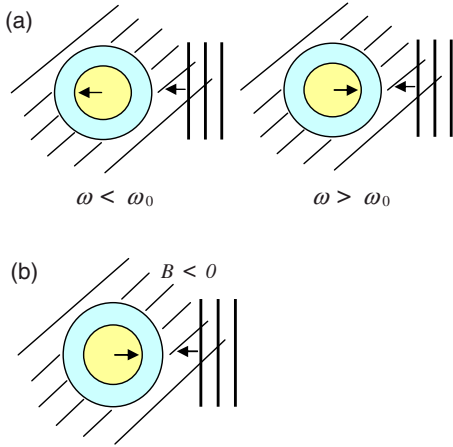


FIG. 12. (Color online) (a) When the core particle oscillation is in phase with the wave in the matrix medium ( $\omega < \omega_0$ ), the dynamic mass density must be positive, as shown on the left. When  $\omega > \omega_0$ , the core particle oscillates out of phase with the wave in the matrix medium, as shown on the right, and the dynamic mass density can be negative provided that the density of coated inclusions is sufficiently high and the core particles have a higher density than that of the matrix medium. (b) Acoustic metamaterial is realized when the dynamic mass density is negative and the fluid medium is also resonant, with negative bulk modulus as a result.

relevance of these results to acoustic metamaterials is clear: Since both bulk modulus and dynamic mass density can be negative, for the realization of acoustic metamaterials it only requires both to occur within the same frequency regime. Recently, the Berkeley group has realized a negative bulk modulus by using HRs. It has thus been proposed that by combining the locally resonant inclusions and the HRs, it may be possible to realize acoustic metamaterials. A schematic picture envisioning this scheme is depicted in Fig. 12.<sup>15</sup>

#### ACKNOWLEDGMENT

We acknowledge the partial support of this work by CA06/07.SC04.

#### APPENDIX A

In this appendix, we evaluate the  $G$  matrix [defined in Eq. (13)] in the long wavelength limit. The structure matrix elements of  $G$  may be expressed as<sup>12</sup>

$$G_{nm}(\vec{k}) = (-1)^l S_{-l}(\alpha_1, \vec{k}), \quad (\text{A1})$$

where  $l = n'' - n$  and  $S_l(\alpha_1, \vec{k})$  is defined as<sup>16</sup>

$$S_l(\alpha_1, \vec{k}) = S_l^J(\alpha_1, \vec{k}) + i S_l^Y(\alpha_1, \vec{k}),$$

$$S_l^J(\alpha_1, \vec{k}) = -\delta_{l,0},$$

$$S_l^Y(\alpha_1, \vec{k}) J_{l+m}(\alpha_1) = - \left[ Y_m(\alpha_1) + \frac{1}{\pi} \sum_{n=1}^m \frac{(m-n)!}{(n-1)!} \left( \frac{2}{\alpha_1} \right)^{m-2n+2} \right] \delta_{l,0} - i \frac{4}{A} \sum_h \left( \frac{\alpha_1}{Q_h} \right)^m \frac{J_{l+m}(Q_h)}{Q_h^2 - \alpha_1^2} e^{il\theta_h}, \quad (\text{A2})$$

in which  $Q_h = |\vec{Q}_h|$ ,  $\theta_h = \arg(\vec{Q}_h)$ ,  $\vec{Q}_h = \vec{K}_h - \vec{k}$ , with  $\vec{K}_h$  being the reciprocal lattice vector and  $\vec{k}$  denoting the reduced wave vector in the first Brillouin zone, and  $Y_n$  being the Neumann function (i.e., Bessel function of the second kind). Here,  $A$  is the unit cell area.

In Eq. (A2),  $m$  is an arbitrary non-negative integer used to improve the convergence of the lattice sum. For convenience, if we set  $m=0$ , then

$$S_l^Y(\alpha_1, \vec{k}) J_l(\alpha_1) = -Y_0(\alpha_1) \delta_{l,0} - i \frac{4}{A} \sum_h \frac{J_l(Q_h)}{Q_h^2 - \alpha_1^2} e^{il\theta_h}. \quad (\text{A3})$$

To obtain the low-frequency dispersion curve, we consider the quasistatic limit of  $|\vec{k}| \rightarrow 0$ . In this limit,  $\alpha_1$  is linearly proportional to  $k$  so that it can be written as  $\alpha_1 = xk \rightarrow 0$  when  $\vec{k} \rightarrow 0$ , in which parameter  $x$  is the constant to be evaluated. It should be noted that  $Q_h \approx K_h$  (for  $K_h \neq 0$ ) and  $\vec{Q}_0 = \vec{k}$  (for  $K_h = 0$ ). Under the dipole approximation, the lattice sums involve orders of 0, 1, and 2 only,<sup>17</sup>

$$S_0^Y(\alpha_1, \vec{k}) \approx -\frac{4}{A} \frac{1}{k^2(1-x^2)} - \frac{2}{\pi} \ln \alpha_1 - \frac{4}{A} \sum_{h \neq 0} \frac{J_0(K_h)}{K_h^2}, \quad (\text{A4})$$

$$S_1^Y(\alpha_1, \vec{k}) \approx -i \frac{4}{A} \frac{1}{k^2 x(1-x^2)} e^{i\theta_0} - i \frac{8}{\alpha_1 A} \sum_{h \neq 0} \frac{J_1(K_h)}{K_h^2} e^{i\theta'_h}, \quad (\text{A5})$$

$$S_2^Y(\alpha_1, \vec{k}) \approx \frac{4}{A} \frac{1}{k^2 x^2(1-x^2)} e^{2i\theta_0} + \frac{32}{\alpha_1^2 A} \sum_{h \neq 0} \frac{J_2(K_h)}{K_h^2} e^{2i\theta'_h}, \quad (\text{A6})$$

where  $\theta_0$  is the polar angle of  $\vec{k}$  and  $\theta'_h = \arg(\vec{K}_h)$ . Generally, for any array of cylinders, the last term on the right-hand side of Eq. (A4) converges to a constant, while the corresponding term in Eq. (A5) vanishes identically. The last term on the right-hand side of Eq. (A6) vanishes only for the square or hexagonal lattice.<sup>17</sup> For simplicity, in what follows we restrict ourselves only to the square or hexagonal lattice. It follows from the above that the dominant terms in Eqs. (A4)–(A6) are

$$S_0^Y(\alpha_1, \vec{k}) \approx -\frac{4}{A} \frac{1}{k^2(1-x^2)}, \quad (\text{A7})$$

$$S_1^Y(\alpha_1, \vec{k}) \approx -i \frac{4}{A} \frac{1}{k^2 x (1-x^2)} e^{i\theta_0}, \quad (\text{A8})$$

$$S_2^Y(\alpha_1, \vec{k}) \approx \frac{4}{A} \frac{1}{k^2 x^2 (1-x^2)} e^{2i\theta_0}. \quad (\text{A9})$$

It is noted that the lattice sums of negative order are given by the complex conjugate of the lattice sums of corresponding positive order,

$$S_{-l}^Y(\alpha_1, \vec{k}) = S_l^{Y*}(\alpha_1, \vec{k}). \quad (\text{A10})$$

After some algebraic manipulations, the  $G$  matrix can be simplified into a  $3 \times 3$  matrix,

$$\begin{aligned} G &= \begin{bmatrix} G_0(\alpha_1) & G_1(\alpha_1) & G_2(\alpha_1) \\ G_{-1}(\alpha_1) & G_0(\alpha_1) & G_1(\alpha_1) \\ G_{-2}(\alpha_1) & G_{-1}(\alpha_1) & G_0(\alpha_1) \end{bmatrix} \\ &= \begin{bmatrix} S_0(\alpha_1, \vec{k}) & -S_{-1}(\alpha_1, \vec{k}) & S_{-2}(\alpha_1, \vec{k}) \\ -S_1(\alpha_1, \vec{k}) & S_0(\alpha_1, \vec{k}) & -S_{-1}(\alpha_1, \vec{k}) \\ S_2(\alpha_1, \vec{k}) & -S_1(\alpha_1, \vec{k}) & S_0(\alpha_1, \vec{k}) \end{bmatrix} \\ &= -I + i \begin{bmatrix} S_0^Y(\alpha_1) & -S_{-1}^Y(\alpha_1) & S_{-2}^Y(\alpha_1) \\ -S_1^Y(\alpha_1) & S_0^Y(\alpha_1) & -S_{-1}^Y(\alpha_1) \\ S_2^Y(\alpha_1) & -S_1^Y(\alpha_1) & S_0^Y(\alpha_1) \end{bmatrix} \end{aligned}$$

$$\approx -I + \frac{4i}{A} \frac{1}{1-x^2} \frac{1}{\alpha_1^2} \begin{bmatrix} -x^2 & xe^{-i\theta_0} & e^{-2i\theta_0} \\ -xe^{i\theta_0} & -x^2 & xe^{-i\theta_0} \\ e^{2i\theta_0} & -xe^{i\theta_0} & -x^2 \end{bmatrix}. \quad (\text{A11})$$

## APPENDIX B

In this appendix, we demonstrate the procedure to obtain the Mie scattering matrix, i.e., the  $T$  matrix, in the low-frequency limit. Suppose the solid cylinders of radius  $r$ , mass density  $D_2$ , and Lamé constants  $\lambda_2$  and  $\mu_2$  are placed in a fluid with corresponding parameter values  $D_1$  and  $\lambda_1$ . Displacement and normal stress continuity at the interface requires that (please see Ref. 12 for details)

$$\begin{aligned} u_{1,\rho}|_{\rho=r} &= u_{2,\rho}|_{\rho=r}, \\ \tau_{1,\rho\rho}|_{\rho=r} &= \tau_{2,\rho\rho}|_{\rho=r}, \\ 0 &= \tau_{2,\rho\phi}|_{\rho=r}, \end{aligned} \quad (\text{B1})$$

which leads to the following equations:

$$\begin{aligned} A_1 a_{n1} + B_1 b_{n1} &= C_{11} c_{n1} + C_{12} c_{n2}, \\ A_2 a_{n1} + B_2 b_{n1} &= C_{21} c_{n1} + C_{22} c_{n2}, \\ 0 &= C_{31} c_{n1} + C_{32} c_{n2}, \end{aligned} \quad (\text{B2})$$

where

$$\begin{aligned} A_1 &= \frac{nJ_n(\alpha_1 r) - \alpha_1 r J_{n+1}(\alpha_1 r)}{r}, \\ B_1 &= \frac{nH_n(\alpha_1 r) - \alpha_1 r H_{n+1}(\alpha_1 r)}{r}, \\ C_{11} &= \frac{nJ_n(\alpha_2 r) - \alpha_2 r J_{n+1}(\alpha_2 r)}{r}, \\ C_{12} &= \frac{inJ_n(\beta_2 r)}{r}, \\ A_2 &= \frac{-\lambda_1(2n+2)\alpha_1 r J_{n+1}(\alpha_1 r) + \lambda_1 \alpha_1^2 r^2 J_{n+2}(\alpha_1 r)}{r}, \\ B_2 &= \frac{-\lambda_1(2n+2)\alpha_1 r H_{n+1}(\alpha_1 r) + \lambda_1 \alpha_1^2 r^2 H_{n+2}(\alpha_1 r)}{r}, \\ C_{21} &= \frac{2\mu_2(n^2 - n)J_n(\alpha_2 r) - [\lambda_2(2n+2) + 2\mu_2(2n+1)]\alpha_2 r J_{n+1}(\alpha_2 r) + (\lambda_2 + 2\mu_2)\alpha_2^2 r^2 J_{n+2}(\alpha_2 r)}{r}, \\ C_{22} &= 2in\mu_2 \frac{(n-1)J_n(\beta_2 r) - \beta_2 r J_{n+1}(\beta_2 r)}{r}, \end{aligned}$$

$$C_{31} = 2in\mu_2 \frac{(n-1)J_n(\alpha_2 r) - \alpha_2 r J_{n+1}(\alpha_2 r)}{r},$$

$$C_{32} = \mu_2 \frac{2(n^2 - n)J_n(\beta_2 r) + 2n\beta_2 r J_{n+1}(\beta_2 r) - \beta_2^2 r^2 J_{n+2}(\beta_2 r)}{r}. \quad (\text{B3})$$

According to the series representation of the Bessel function,<sup>18</sup> we have

$$J_n(z) = \frac{z^n}{2^n} \sum_{k=0}^{\infty} (-1)^k \frac{z^{2k}}{2^{2k} k! \Gamma(n+k+1)},$$

$$\pi N_n(z) = 2J_n(z) \ln \frac{z}{2} - \sum_{k=0}^{n-1} \frac{(n-k-1)!}{k!} \left(\frac{z}{2}\right)^{2k-n}$$

$$- \sum_{k=0}^{\infty} (-1)^k \frac{1}{k!(k+n)!} \left(\frac{z}{2}\right)^{n+2k}$$

$$\times [\psi(k+1) + \psi(k+n+1)], \quad (\text{B4})$$

where  $\psi(x)$  is the psi function. In order to evaluate the scattering matrix at the low-frequency limit  $\alpha \rightarrow 0$  or  $\beta \rightarrow 0$ , we retain only two leading-order terms in the Bessel function series expansions,

$$J_1(\alpha_1 r) \rightarrow \frac{1}{2} r \alpha_1 - \frac{1}{16} r^3 \alpha_1^3,$$

$$J_2(\alpha_1 r) \rightarrow \frac{1}{8} r^2 \alpha_1^2 - \frac{1}{96} r^4 \alpha_1^4,$$

$$J_3(\alpha_1 r) \rightarrow \frac{1}{48} r^3 \alpha_1^3 - \frac{1}{768} r^5 \alpha_1^5,$$

$$\dots$$

$$H_1(\alpha_1 r) \rightarrow \frac{1}{2} r \alpha_1 - \frac{1}{16} r^3 \alpha_1^3 - i \frac{2}{\pi} \frac{1}{r \alpha_1} + i \frac{\gamma_0 - \frac{1}{2}}{\pi} r \alpha_1,$$

$$H_2(\alpha_1 r) \rightarrow \frac{1}{8} r^2 \alpha_1^2 - \frac{1}{96} r^4 \alpha_1^4 - i \frac{4}{\pi} \frac{1}{r^2 \alpha_1^2} - i \frac{1}{\pi},$$

$$H_3(\alpha_1 r) \rightarrow \frac{1}{48} r^3 \alpha_1^3 - \frac{1}{768} r^5 \alpha_1^5 - i \frac{16}{\pi} \frac{1}{r^3 \alpha_1^3} - i \frac{2}{\pi} \frac{1}{r \alpha_1},$$

$$\dots, \quad (\text{B5})$$

where  $\gamma_0 \approx 0.577 215$  denotes the Euler constant.

Since  $a_n = \sum_{n'} (T^{-1})_{nn'} b_{n'}$ , according to Eq. (B2), we can arrive at

$$(T^{-1})_{nn'} = \frac{(C_{11}C_{32} - C_{12}C_{31})B_2 - (C_{21}C_{32} - C_{22}C_{31})B_1}{(C_{21}C_{32} - C_{22}C_{31})A_1 - (C_{11}C_{32} - C_{12}C_{31})A_2} \delta_{nn'}. \quad (\text{B6})$$

It turns out that for the  $n=0$  angular scattering channel,

$$(T^{-1})_{00} \rightarrow -1 + \frac{4i}{\pi r^2} \frac{\lambda_2 + \mu_2}{\lambda_2 + \mu_2 - \lambda_1} \frac{1}{\alpha_1^2},$$

while for the  $n=\pm 1$  angular scattering channels,

$$(T^{-1})_{nm} \rightarrow -1 + \frac{4i}{\pi r^2} \frac{D_1 + D_2}{D_1 - D_2} \frac{1}{\alpha_1^2}.$$

So, we finally obtain the  $T$  matrix limiting behavior as

$$T^{-1} = -I + \frac{4i}{\pi r^2} \frac{1}{\alpha_1^2} \begin{bmatrix} \frac{D_1 + D_2}{D_1 - D_2} & 0 & 0 \\ 0 & \frac{\lambda_2 + \mu_2}{\lambda_2 + \mu_2 - \lambda_1} & 0 \\ 0 & 0 & \frac{D_1 + D_2}{D_1 - D_2} \end{bmatrix}. \quad (\text{B7})$$

## APPENDIX C

In this appendix, we evaluate the  $T^{-1}-G$  matrix for the case of the solid matrix in the long wavelength limit. We first note that the  $G$  matrix for the transverse  $z$  mode should have almost the same form as Eq. (A11). The only difference between the two is that for the  $G$  matrix of the transverse  $z$  mode, we should replace each  $\alpha_1 = \omega \sqrt{D_1/\lambda_1}$  in Eq. (A11) with  $\beta_1 = \omega \sqrt{D_1/\mu_1}$  to obtain

$$G = -I + \frac{4i}{A} \frac{1}{1-x^2} \frac{1}{\beta_1^2} \begin{bmatrix} -x^2 & xe^{-i\theta_0} & e^{-2i\theta_0} \\ -xe^{i\theta_0} & -x^2 & xe^{-i\theta_0} \\ e^{2i\theta_0} & -xe^{i\theta_0} & -x^2 \end{bmatrix} \quad (\text{C1})$$

because we are now concerned with the transverse mode instead of the longitudinal mode.

For the  $T$  matrix, let us assume that the solid cylinders of radius  $r$ , mass density  $D_2$ , and Lamé constants  $\lambda_2$  and  $\mu_2$  are now embedded in a solid matrix with mass density  $D_1$  and Lamé constants  $\lambda_1$  and  $\mu_1$ . Displacement and tangential stress continuity at the interface requires that (see Ref. 12 for details)

$$\begin{aligned} u_{1,z}|_{\rho=r} &= u_{2,z}|_{\rho=r}, \\ \tau_{1,\rho z}|_{\rho=r} &= \tau_{2,\rho z}|_{\rho=r}, \end{aligned} \quad (\text{C2})$$

$$\begin{aligned} A_1 a_{n3} + B_1 b_{n3} &= C_1 c_{n3}, \\ A_2 a_{n3} + B_2 b_{n3} &= C_2 c_{n3}, \end{aligned} \quad (\text{C3})$$

which leads to the following equations:

where

$$\begin{aligned} A_1 &= \frac{(2n+2)J_{n+1}(\beta_1 r) - \beta_1 r J_{n+2}(\beta_1 r)}{r}, \\ B_1 &= \frac{(2n+2)H_{n+1}(\beta_1 r) - \beta_1 r H_{n+2}(\beta_1 r)}{r}, \\ C_1 &= \frac{(2n+2)J_{n+1}(\beta_2 r) - \beta_2 r J_{n+2}(\beta_2 r)}{r}, \\ A_2 &= \mu_1 \frac{2n(n+1)J_{n+1}(\beta_1 r) - (3n+4)\beta_1 r J_{n+2}(\beta_1 r) + \beta_1^2 r^2 J_{n+3}(\beta_1 r)}{r}, \\ B_2 &= \mu_1 \frac{2n(n+1)H_{n+1}(\beta_1 r) - (3n+4)\beta_1 r H_{n+2}(\beta_1 r) + \beta_1^2 r^2 H_{n+3}(\beta_1 r)}{r}, \\ C_2 &= \mu_2 \frac{2n(n+1)J_{n+1}(\beta_2 r) - (3n+4)\beta_2 r J_{n+2}(\beta_2 r) + \beta_2^2 r^2 J_{n+3}(\beta_2 r)}{r}. \end{aligned} \quad (\text{C4})$$

According to Eq. (C3), elements of the inverse  $T$  matrix are given by

$$(T^{-1})_{nm'} = \frac{B_2 C_1 - B_1 C_2}{A_1 C_2 - A_2 C_1} \delta_{nm'}. \quad (\text{C5})$$

By retaining two leading-order terms in the series expansions of Bessel and Hankel functions, we get for the  $n=0$  channel

$$(T^{-1})_{00} \rightarrow -1 + \frac{4i}{\pi r^2} \frac{D_1}{D_1 - D_2} \frac{1}{\beta_1^2},$$

while for the  $n=\pm 1$  channels

$$(T^{-1})_{nn} \rightarrow -1 + \frac{4i}{\pi r^2} \frac{\mu_2 + \mu_1}{\mu_2 - \mu_1} \frac{1}{\beta_1^2}.$$

So, we would arrive at the limiting form of the  $T$  matrix as

$$T^{-1} = -I + \frac{4i}{\pi r^2} \frac{1}{\beta_1^2} \begin{bmatrix} \frac{\mu_2 + \mu_1}{\mu_2 - \mu_1} & 0 & 0 \\ 0 & \frac{D_1}{D_1 - D_2} & 0 \\ 0 & 0 & \frac{\mu_2 + \mu_1}{\mu_2 - \mu_1} \end{bmatrix}. \quad (\text{C6})$$

<sup>1</sup>G. T. Kuster, and M. N. Toksöz, *Geophysics* **39**, 587 (1974).

<sup>2</sup>J. G. Berryman, *J. Acoust. Soc. Am.* **68**, 1809 (1980); **68**, 1820 (1980).

<sup>3</sup>P. Sheng, X. X. Zhang, Z. Liu, and C. T. Chan, *Physica B* **338**, 201 (2003).

<sup>4</sup>Z. Liu, X. X. Zhang, Y. Mao, Y. Y. Zhu, Z. Yang, C. T. Chan, and P. Sheng, *Science* **289**, 1641 (2000).

<sup>5</sup>Z. Liu, C. T. Chan, and P. Sheng, *Phys. Rev. B* **71**, 014103 (2005).

<sup>6</sup>J. Mei, Z. Liu, W. Wen, and P. Sheng, *Phys. Rev. Lett.* **96**, 024301 (2006).

<sup>7</sup>F. Cervera, L. Sanchis, J. V. Sánchez-Pérez, R. Martínez-Sala, C. Rubio, F. Meseguer, C. López, D. Caballero, and J. Sánchez-Dehesa, *Phys. Rev. Lett.* **88**, 023902 (2001).

<sup>8</sup>G. W. Milton and J. R. Willis, *Proc. R. Soc. London, Ser. A* **463**, 855 (2007).

<sup>9</sup>A. Áliva, G. Griso, and B. Miara, *C. R. Math.* **340**, 933 (2005).

<sup>10</sup>N. Fang, D. Xi, J. Xu, M. Ambati, W. Sritravanich, C. Sun, and

- X. Zhang, *Nat. Mater.* **5**, 452 (2006).
- <sup>11</sup>P. Sheng, *Introduction to Wave Scattering, Localization and Mesoscopic Phenomena*, 2nd ed. (Springer, Berlin, 2006), Chap. 4.
- <sup>12</sup>J. Mei, Z. Liu, J. Shi, and D. Tian, *Phys. Rev. B* **67**, 245107 (2003).
- <sup>13</sup>Y. Wu, J. Li, Z. Q. Zhang, and C. T. Chan, *Phys. Rev. B* **74**, 085111 (2006).
- <sup>14</sup>J. Li and C. T. Chan, *Phys. Rev. E* **70**, 055602(R) (2004).
- <sup>15</sup>P. Sheng, J. Mei, Z. Liu, and W. Wen, *Physica B* **394**, 256 (2007).
- <sup>16</sup>S. K. Chin, N. A. Nicorovici, and R. C. McPhedran, *Phys. Rev. E* **49**, 4590 (1994).
- <sup>17</sup>N. A. Nicorovici, R. C. McPhedran, and L. C. Botten, *Phys. Rev. E* **52**, 1135 (1995).
- <sup>18</sup>I. S. Gradshteyn and I. M. Ryzhik, *Table of Integrals, Series, and Products* (Academic, New York, 1965).